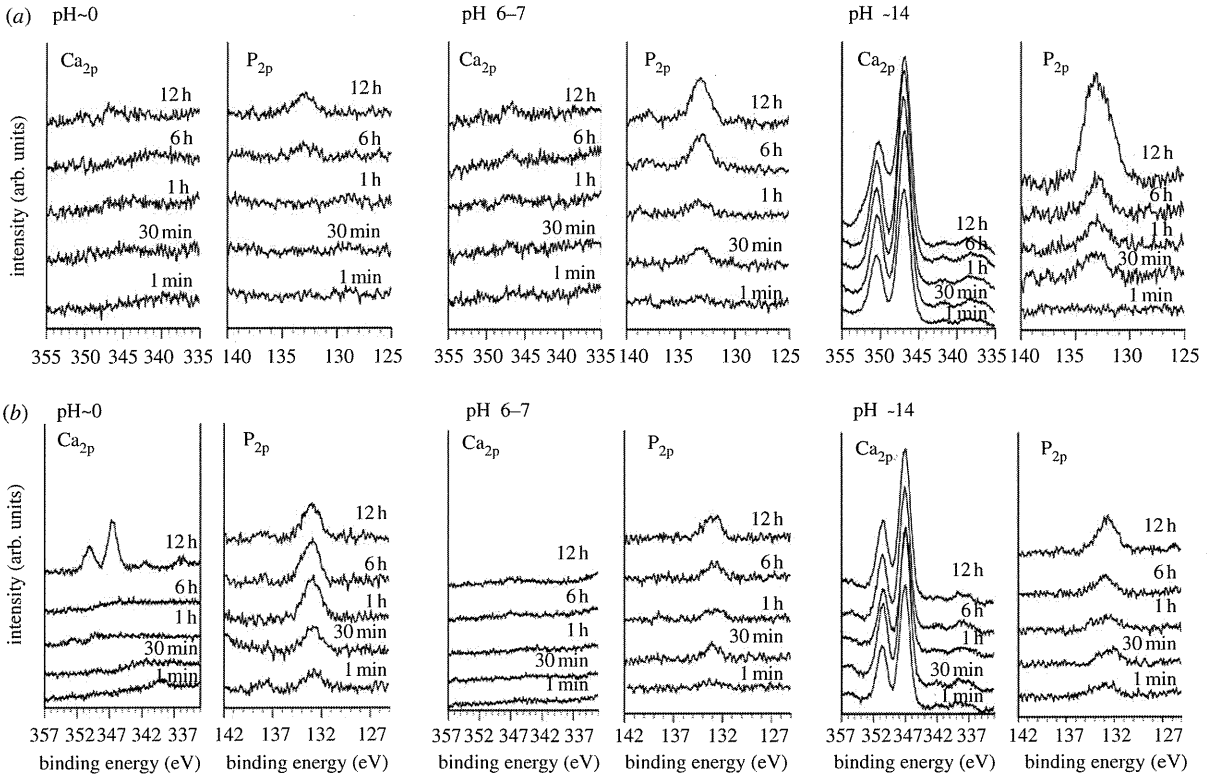

Figure 7. (*a*) XPS spectra of surfaces of Ti as exposed to solutions with pHs approximately 0, 6–7 and 14, and (*b*) those subsequent heat-treated as a function of soaking time in SBF.

Ti specimens exposed to solutions with an intermediate pH that ranged from 3.4 to 12.9 did not form any apatite, even after the heat treatment.

3.5. *X-ray photoelectron spectroscopy spectra of the treated Ti metal*

Figure 7 shows the Ca_{2P} and P_{2P} XPS spectra of the Ti surfaces exposed to solutions of pH values of approximately 0, 6–7 and 14 and those subsequently heat-treated as a function of soaking time in SBF. It can be seen that Ti specimens before heat treatment adsorb a small amount of the calcium and phosphate ions almost simultaneously, independent of pH, except in cases of a high pH, where it first selectively adsorbs the calcium ions, and then the phosphate ions.

In contrast, Ti specimens exposed to a low pH solution and subsequently heat-treated first selectively adsorb phosphate ions and then the calcium ions, whereas those exposed to a high pH and subsequently heat-treated do the opposite, i.e. first selectively adsorbing calcium ions and then phosphate ions. Ti specimens exposed to an intermediate pH adsorb a small amount of the calcium and phosphate ions almost simultaneously, even after the heat treatment.

4. DISCUSSION

It is apparent from figures 5 and 6 that the Ti specimens did not form surface apatite in SBF when exposed to the solutions, except when it was exposed to a strongly alkaline solution, which resulted in a small amount of apatite formation, whereas those that were subsequently heat-treated exhibited a large amount of apatite after exposure to strongly acidic or alkaline solutions.

Micrometre or nanometre scale roughness was produced on Ti specimens when they were exposed to strongly acidic or alkaline solutions, and this was not changed by the subsequent heat treatment, as shown in figure 1. This indicates that the surface morphology is not responsible for the increased apatite formation induced by the heat treatment. It should be emphasized that even the highly porous surface formed by the NaOH treatment was not responsible for apatite formation, because the highly porous surface was apparently not changed by the subsequent heat treatment, whereas the apatite formation was remarkably increased by the heat treatment, as shown by higher density of the apatite for heat-treated specimen on FE-SEM picture in figure 5.

TH or SHT was precipitated on Ti specimens when they were exposed to strongly acidic or alkaline solutions, and the precipitate was transformed into rutile or sodium titanate accompanied by rutile upon subsequent heat treatment (figure 2). This suggests that the rutile and sodium titanate are responsible for the increased apatite formation induced by the heat treatment. However, rutile was also detected on heat-treated Ti specimens after exposure to solutions with intermediate pH values (figure 2), which did not form the apatite. This indicates that the composition and structure of the rutile phase is not responsible for the increase in apatite formation induced by the heat treatment.

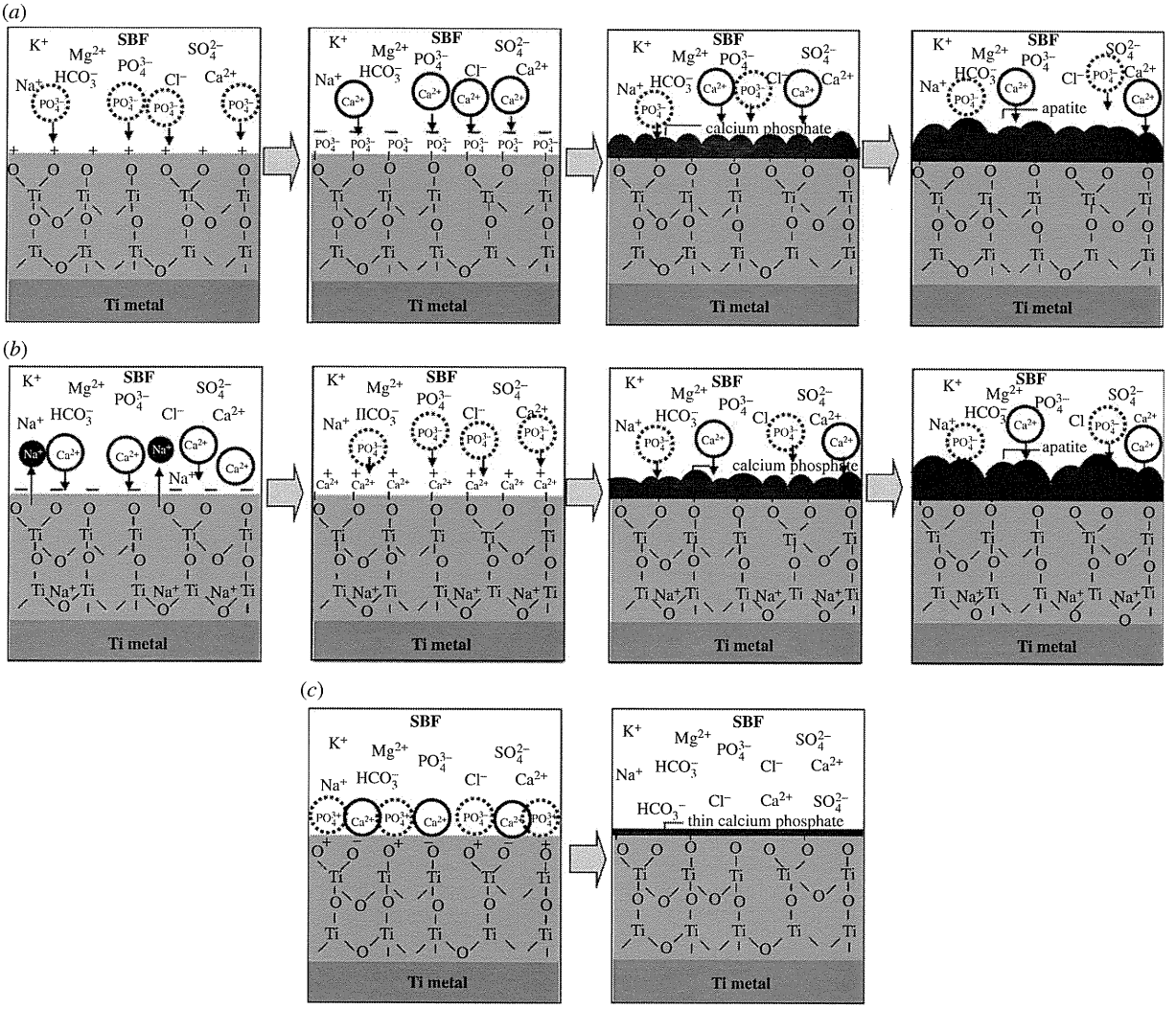

Figure 8. Schematic of ion adsorption on (*a*) positively charged, (*b*) negatively charged and (*c*) neutrally charged Ti metal.

The Ti specimens exposed to the solutions displayed a zeta potential of approximately zero, independent of the pH of the exposed solution, whereas those that were subsequently heat-treated displayed a certain level of positive or negative zeta potential when they were exposed to a strongly acidic or alkaline solution, respectively. This indicates that the certain level of the positive or negative surface charges is responsible for the apatite formation induced by the heat treatment. It is suggested that the positively charged surface first selectively adsorbs the negatively charged phosphate ions on its surface. As the phosphate ions accumulate, the surface becomes negatively charged. As a result, the positively charged calcium ions are adsorbed on its surface so as to produce a calcium phosphate which is eventually transformed into apatite, as shown in figure 8*a*. On the other hand, the negatively charged surface is assumed to first selectively adsorb positively charged calcium ions and then the negatively charged phosphate ions so as to also form apatite, as shown in figure 8*b*.

It is shown by the XPS spectra in figure 7 that the former type of phosphate and calcium ion adsorption occurred on heat-treated Ti specimens after exposure to strongly acidic solutions, while the latter type of sequential adsorption occurred on heat-treated Ti specimens after the strongly alkaline solutions.

The Ti specimen that was heat-treated after exposure to solutions with intermediate pH values exhibited a zeta potential of almost zero (figure 3). This means that the positively and negatively charged sites are balanced and hence the surface is neutrally charged [30]. It is assumed that each Ti site is able to simultaneously adsorb negatively charged phosphate ions and positively charged calcium ions, respectively, as shown in figure 8*c*. As a result, a thin calcium phosphate layer is formed on their surfaces and their charges are soon neutralized, and hence the calcium phosphate layer does not grow into the thick apatite layer in a short period of time. It is also evident from the XPS spectra in figure 7 that this type of simultaneous adsorption of the small amount of the phosphate and calcium ions occurred on Ti specimens that were heat-treated after exposure to solutions with intermediate pH value. However, the calcium phosphate layer was so thin that it was not apparently observed under FE-SEM with the

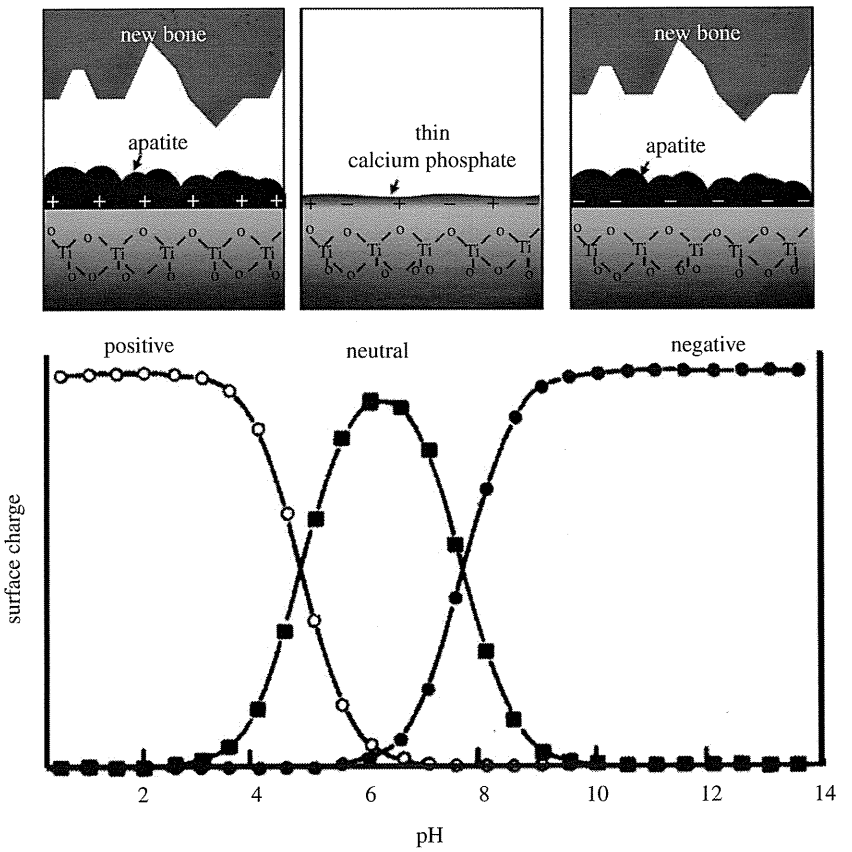

Figure 9. Apatite formation and bone-bonding of Ti as a function of pH of exposed solution. Lower part of this figure was reproduced from Textor *et al.* [30] after modification.

resolution of several nanometres in figure 5, and precipitation of apatite on the specimens was not detected by TF-XRD patterns in figure 6. The apatite formation on heat-treated Ti specimens after strong acid or alkali solutions is thus attributed to their positive or negative surface charges, respectively.

The reason why Ti specimens that are heat-treated after exposure to the strong acid solutions are charged positively may be due to the titanium oxide adsorbed with the Cl^- ions on their surfaces. It is assumed that the Cl^- ions were adsorbed on the TH on the surface of the Ti specimens when they were exposed to the strong acid solutions, and they remained on the titanium oxide that was formed on the Ti specimens by the subsequent heat treatment. The adsorption of the Cl^- ions on the TH on the Ti specimens exposed to the acid solutions and the adsorption of those on the titanium oxide on Ti specimens that were subsequently heat-treated were demonstrated by the GD-OES spectra shown in figure 4. These adsorbed Cl^- ions may become dissociated via exchange with OH^- ions in SBF so as to give rise to an acidic environment. It has been reported by Textor *et al.* [30] that titanium oxide is positively charged by forming larger numbers of $Ti\text{-}OH_2^+$ groups in acidic solutions. A recent report has shown that the positive charge and apatite formation on the Ti metal can be induced by not only Cl^-, but also other acid radicals such as NO_3^- and SO_4^{2-} [31].

The reason why Ti specimens that are heat-treated after exposure to strongly alkaline solutions are charged negatively may be due to the sodium titanate on their surfaces. The sodium titanate releases its Na^+ ions via exchange with the H_3O^+ ions in SBF to form Ti-OH groups on its surface [32–35] by the following reaction

$$\mathrm{Ti-ONa(metal)} + \mathrm{H_2O(SBF)} \rightarrow \mathrm{Ti-OH(metal)} + \mathrm{OH^-(SBF)} + \mathrm{Na^+(SBF)}$$

This increases the pH of the surrounding SBF because of the consumption of H_3O^+ ions. It has been reported by Textor *et al.* [30] that titanium oxide is negatively charged by forming $Ti\text{-}O^-$ groups in alkaline solution.

In the case of the Ti specimens prior to heat treatment, they became covered with a thin titanium oxide layer when they were exposed to the solutions with intermediate pH values, similar to the untreated Ti specimen. This titanium oxide layer has an almost neutral surface charge (figure 3) and hence does not induce the apatite formation. They did form TH on their surfaces when they were exposed to the strongly acidic solutions. This phase is electrically conductive [36]. Therefore, their surfaces are hardly charged even though they adsorbed Cl^- ions, and hence did not induce the apatite formation.

Ti specimens formed an SHT on their surfaces upon exposure to strongly alkaline solutions. The SHT also releases its Na^+ ions via exchange with H_3O^+ ions in

SBF to form negatively charged Ti-OH groups [37]. However, SHT is electrically conductive, and hence its negative surface charge is so small that it cannot be measured by the present method. Therefore, Ti specimens exposed to the strongly alkaline solution induced apatite formation, but its magnitude was smaller than that of the Ti specimen that was subsequently heat-treated, as shown in figure 5. It is apparent from these findings that the Ti specimen that is heat-treated after exposure to a strongly acidic or alkaline solution can induce surface apatite formation in SBF, because of its large positive or negative surface charges.

It has been shown for various kinds of ceramics, including glasses, glass-ceramics and sintered crystalline ceramics of various compositions, that materials that have the capacity to form a surface apatite layer in the living body are able to bond to living bone through the apatite layer [27], and are useful as long as they contain neither cytotoxic nor antigenic components, and furthermore, their apatite formation can be reproduced even in an acellular SBF having ion concentrations almost equal to those of human blood plasma [27]. Bohner *et al.* [38] and Pan *et al.* [39] recently pointed out that certain resorbable ceramics bond to living bone without any formation of a surface apatite layer. These exceptional cases were also pointed out in the paper described earlier [27]. This means that the rule described earlier should be applied with caution in the case of resorbable materials. However, Ti is not a resorbable material, and contains neither cytotoxic nor antigenic components. It has already been shown that Ti and various kinds of Ti-based alloys (such as Ti–6Al–4V, Ti–15Mo–5Zr–3Al and Ti–15Zr–4Nb–4Ta) that are able to form apatite on their surfaces in SBF, bond to living bone through the apatite layer formed on their surfaces in the living body [23,24,26,40–47].

In view of these findings, it is predicted from the present results that Ti forms a bone-like apatite surface layer in the living body and bonds to living bone through the apatite layer upon exposure to a strongly acidic or alkaline solution and then heat-treated, because its surface is then either positively or negatively charged in the living body. In contrast with this, Ti exposed to solutions with intermediate pH values and subsequently subjected to the heat treatment forms only a thin amorphous calcium phosphate layer in the living body, and hence possesses a good compatibility with the bone but does not bond to bone, because the surface is almost neutrally charged, as shown in figure 9. The Ti not subjected to heat treatment after the solution treatment displayed little or no surface apatite formation in the living body, and hence do not bond to living bone, because their surfaces are almost entirely neutrally charged.

5. CONCLUSION

Ti specimens that were heat-treated after exposure to strong acid or alkali solutions showed remarkable apatite formation on their surfaces in SBF, while those heat-treated after exposure to solutions with intermediate pHs did not show any such apatite formation.

The remarkable apatite formation of Ti exposed to the strongly acidic and alkaline solutions is attributed to the magnitude of their positive and negative surface charges, respectively. The positive and negative surface charges are produced by the dissociated chloride ions and the released sodium ions, respectively. The lack of apatite formation on the Ti exposed to intermediate pH solutions is attributed to their neutral surface charges. Ti that were not subjected to heat treatment after the solutions showed no or only a little apatite formation on their surfaces in SBF because of their neutral surface charge.

It is predicted from the present results that the bone-bonding property of Ti strongly depends upon the pH of the solution used, i.e. Ti forms bone-like apatite on its surface in the living body and bonds to living bone through the apatite layer, if it is heat-treated after exposure to a strongly acidic or alkaline solution.

REFERENCES

1 Brunette, D. M., Tengvall, P., Textor, M. & Thomsen, P. 2001 *Titanium in medicine.* Berlin, Germany: Springer.

2 Yan, W. Q., Nakamura, T., Kobayashi, M., Kim, H. M., Miyaji, F. & Kokubo, T. 1997 Bonding of chemically treated titanium implants to bone. *J. Biomed. Mater. Res.* **37**, 267–275. (doi:10.1002/(SICI)1097-4636(199711)37:2, 267::AID-JBM17.3.0.CO;2-B)

3 Hanawa, T., Kamimura, Y., Yamamoto, S., Kohgo, T., Amemiya, A., Ukai, M., Murakami, K. & Asaoka, K. 1997 Early bone formation around calcium-ion-implanted titanium inserted into rat tibia. *J. Biomed. Mater. Res.* **36**, 131–136. (doi:10.1002/(SICI)1097-4636(199707)36: 1<131::AID-JBM16>3.0.CO;2-L)

4 Armitage, D. A., Mihoc, R., Tate, T. J., McPhail, D. S., Chater, R., Hobkirk, J. A., Shinawi, L. & Jones, F. H. 2007 The oxidation of calcium implanted titanium in water: a depth profiling study. *Appl. Surf. Sci.* **253**, 4085–4093. (doi:10.1016/j.apsusc.2006.09.006)

5 Nayab, H., Jones, F. H. & Olsen, I. 2007 Effects of calcium ion-implantation of titanium on bone cell function *in vitro*. *J. Biomed. Mater. Res.* **83A**, 296–302. (doi:10.1002/jbm.a.31218)

6 Sul, Y. T. 2003 The significance of the surface properties of oxidized titanium to the bone response: special emphasis on potential biochemical bonding of oxidized titanium implant. *Biomaterials* **24**, 3893–3907. (doi:10.1016/S0142-9612(03)00261-8)

7 Song, W. H., Ryu, H. S. & Hong, S. H. 2005 Apatite induction on Ca-containing titania formed by micro-arc oxidation. *J. Am. Ceram. Soc.* **88**, 2642–2644. (doi:10.1111/j.1551-2916.2005.00476.x)

8 Frojd, V., Franke-Stenport, V., Meirelles, L. & Wennerberg, A. 2008 Increased bone contact to a calcium-incorporated oxidized commercially pure titanium implant: an *in-vivo* study in rabbits. *Int. J. Oral Maxillofac. Surg.* **37**, 561–566. (doi:10.1016/j.ijom.2008.01.020)

9 Wu, J., Liu, Z. M., Zhao, X. H., Gao, Y., Hu, J. & Gao, B. 2010 Improved biological performance of microarc-oxidized low-modulus Ti-24Nb-4Zr-7.9Sn alloy. *J. Biomed. Mater. Res.* **92B**, 298–306. (doi:10.1002/jbm.b.31515)

10 Whiteside, P., Matykina, E., Gough, J. F., Skeldon, P. & Thompson, G. E. 2010 *In vitro* evaluation of cell proliferation and collagen synthesis on titanium following plasma electrolytic oxidation. *J. Biomed. Mater. Res.* **94A**, 38–46. (doi:10.1002/jbm.a.32664)

11 Nakagawa, M., Zhang, L., Udoh, K., Matsuya, S. & Ishikawa, K. 2005 Effects of hydrothermal treatment with $CaCl_2$ solution on surface property and cell response of titanium implants. *J. Mater. Sci., Mater. Med.* **16**, 985–991. (doi:10.1007/s10856-005-4753-0)

12 Park, J. W., Park, K. B. & Suh, J. Y. 2007 Effects of calcium ion incorporation on bone healing of Ti6Al4V alloy implants in rabbit tibiae. *Biomaterials* **28**, 3306–3313. (doi:10.1016/j.biomaterials.2007.04.007)

13 Ueda, M., Ikeda, M. & Ogawa, M. 2009 Chemical–hydrothermal combined surface modification of titanium for improvement of osteointegration. *J. Mater. Sci. Eng. C* **29**, 994–1000. (doi:10.1016/j.msec.2008.09.002)

14 Chen, X. B., Li, Y. C., Plessis, J. D., Hodgson, P. D. & Wen, C. 2009 Influence of calcium ion deposition on apatite-inducing ability of porous titanium for biomedical applications. *Acta Biomater.* **5**, 1808–1820. (doi:10.1016/j.actbio.2009.01.015)

15 Park, J. W., Kim, Y. J., Jang, J. H., Kwon, T. G., Bae, Y. C. & Suh, J. Y. 2010 Effects of phosphoric acid treatment of titanium surfaces on surface properties, osteoblast response and removal of torque forces. *Acta Biomater.* **6**, 1661–1670. (doi:10.1016/j.actbio.2009.10.011)

16 Wang, X. X., Hayakawa, S., Tsuru, K. & Osaka, A. 2002 Bioactive titania gel layers formed by chemical treatment of Ti substrate with a H_2O_2/HCl solution. *Biomaterials* **23**, 1353–1357. (doi:10.1016/S0142-9612(01)00254-X)

17 Wang, X. X., Yan, W., Hayakawa, S., Tsuru, K. & Osaka, A. 2003 Apatite deposition on thermally and anodically oxidized titanium surfaces in a simulated body fluid. *Biomaterials* **24**, 4631–4637. (doi:10.1016/S0142-9612(03)00357-0)

18 Wu, J. M., Hayakawa, S., Tsuru, K. & Osaka, A. 2004 Low temperature preparation of anatase and rutile layers on titanium substrates and their ability to induce *in vitro* apatite deposition. *J. Am. Ceram. Soc.* **87**, 1635–1642. (doi:10.1111/j.1551-2916.2004.01635.x)

19 Lu, X., Wang, Y., Yang, X., Zhang, Q., Zhao, Z., Weng, L. T. & Leng, Y. 2008 Spectroscopic analysis of titanium surface functional groups under various surface modification and their behaviors *in vitro* and *in vivo*. *J. Biomed. Mater. Res.* **84A**, 523–534. (doi:10.1002/jbm.a.31471)

20 Sugino, A., Ohtsuki, C., Tsuru, K., Hayakawa, S., Nakano, T., Okazaki, Y. & Osaka, A. 2009 Effect of spatial design and thermal oxidation on apatite formation on Ti–15Zr–4Ta–4Nb alloy. *Acta Biomater.* **5**, 298–304. (doi:10.1016/j.actbio.2008.07.014.)

21 Karthega, M. & Rajendran, N. 2010 Hydrogen peroxide treatment on Ti–6Al–4V alloy: a promising surface modification technique for orthopaedic application. *Appl. Surf. Sci.* **256**, 2176–2183. (doi:10.1016/j.apsusc.2009.09.069)

22 Kokubo, T., Miyaji, F., Kim, H. M. & Nakamura, T. 1996 Spontaneous formation of bonelike apatite layer on chemically treated titanium metals. *J. Am. Ceram. Soc.* **79**, 1127–1129. (doi:10.1111/j.1151-2916.1996.tb08561.x)

23 Kim, H. M., Miyaji, F., Kokubo, T. & Nakamura, T. 1996 Preparation of bioactive Ti and its alloy via simple chemical surface treatment. *J. Biomed. Mater. Res.* **32**, 409–417. (doi:10.1002/(SICI)1097-4636(199611)32:3<409:: AID-JBM14>3.0.CO;2-B)

24 Nishiguchi, S., Fujibayashi, S., Kim, H. M., Kokubo, T. & Nakamura, T. 2003 Biology of alkali- and heat-treated titanium implants. *J. Biomed. Mater. Res.* **67A**, 26–35. (doi:10.1002/jbm.a.10540)

25 Kawanabe, K., Ise, K., Goto, K., Akiyama, H., Nakamura, T., Kaneuji, A., Sugimori, T. & Matsumoto, T. 2009 A new cementless total hip arthoplasty with bioactive titanium porous-coating by alkaline and heat treatment: average 4.8-year results. *J. Biomed. Mater. Res.* **90B**, 476–481. (doi:10.1002/jbm.b.31309)

26 Kokubo, T., Pattanayak, D. K., Yamaguchi, S., Takadama, H., Matsushita, T., Kawai, T., Takemoto, M., Fujibayashi, S. & Nakamura, T. 2010 Positively charged bioactive Ti metal prepared by simple chemical and heat treatments. *J. R. Soc. Interface* **7**, S503–S513. (doi:10.1098/rsif.2010.0129.focus)

27 Kokubo, T. & Takadama, H. 2006 How useful is SBF in predicting *in vivo* bone bioactivity? *Biomaterials* **27**, 2907–2915. (doi:10.1016/j.biomaterials.2006.01.017)

28 Sun, X. & Li, Y. 2003 Synthesis and characterization of ion-exchangeable titanate nanotubes. *Chem. Eur. J.* **9**, 2229–2238. (doi:10.1002/chem.200204394)

29 Kim, H.-M., Miyaji, F., Kokubo, T., Nishiguchi, S. & Nakamura, T. 1999 Graded surface structure of bioactive titanium prepared by chemical treatment. *J. Biomed. Mater. Res.* **45**, 100–107. (doi:10.1002/(SICI)1097-4636(199905)45:2<100::AID-JBM4>3.0.CO;2-0)

30 Textor, M., Sittig, C., Frauchiger, V., Tosatti, S. & Brunette, D. M. 2001 Properties and biological significance of natural oxide films on titanium and its alloys. In *Titanium in medicine* (eds D. M. Brunette, P. Tengvall, M. Textor & P. Thomsen), pp. 171–230. Berlin, Germany: Springer.

31 Pattanayak, D. K., Yamaguchi, S., Matsushita, T. & Kokubo, T. 2011 Nanostructured positively charged bioactive TiO_2 layer formed on Ti metal by NaOH, acid and heat treatments. *J. Mater. Sci: Mater. Med.* **22**, 1803–1812. (doi:10.1007/s10856-011-4372-x)

32 Kawai, T., Kizuki, T., Takadama, T., Matsushita, T., Unuma, H., Nakamura, T. & Kokubo, T. 2010 Apatite formation on surface titanate layer with different Na content on Ti metal. *J. Ceram. Soc. Japan* **118**, 19–24.

33 Takadama, H., Kim, H.-M., Kokubo, T. & Nakamura, T. 2001 An X-ray photoelectron spectroscopy study of the process of apatite formation on bioactive titanium metal. *J. Biomed. Mater. Res.* **55**, 185–193. (doi:10.1002/1097-4636(200105)55:2<185::AID-JBM1005>3.0.CO;2-P)

34 Takadama, H., Kim, H.-M., Kokubo, T. & Nakamura, T. 2001 TEM-EDX study of mechanism of bonelike apatite formation on bioactive titanium metal in simulated body fluid. *J. Biomed. Mater. Res.* **57**, 441–448. (doi:10.1002/1097-4636(20011205)57:3<441::AID-JBM1187>3.0.CO;2-B)

35 Kim, H. M., Himeno, T., Kawashita, M., Lee, J. H., Kokubo, T. & Nakamura, T. 2003 Surface potential change in bioactive titanium metal during the process of apatite formation in simulated body fluid. *J. Biomed. Mater. Res. A* **67**, 1305–1309. (doi:10.1002/jbm.a.20039)

36 Ito, M., Setoyama, D., Matsunaga, J., Muta, H., Kurosaki, K., Masayoshi, U. & Yamanaka, S. 2006 Electrical and thermal properties of titanium hydrides. *J. Alloys Compd.* **420**, 25–28. (doi:10.1016/j.jallcom.2005.10.032)

37 Kim, H.-M., Miyaji, F., Kokubo, T. & Nakamura, T. 1997 Apatite-forming ability of alkali-treated Ti metal in body environment. *J. Ceram. Soc. Japan* **105**, 111–116.

38 Bohner, M. & Lemahitre, J. 2009 Can bioactivity be tested *in vitro* with SBF solution? *Biomaterials* **30**, 2175–2179. (doi:10.1016/j.biomaterials.2009.01.008)

39 Pan, H., Zhao, X., Darvell, B. W. & Lu, W. W. 2010 Apatite-formation ability: predictor of 'bioactivity'? *Acta Biomater.* **6**, 4181–4188. (doi:10.1016/j.actbio.2010.05.013)

40 Nishiguchi, S., Kato, H., Fujita, H., Kim, H. M., Miyaji, F., Kokubo, T. & Nakamura, T. 1999 Enhancement of bone-bonding strengths of titanium alloy implants by alkali and heat treatments. *J. Biomed. Mater. Res.* (*Appl Biomater.*) **48**, 689–696. (doi:10.1002/(SICI)1097-4636(1999)48:5<689::AID-JBM13>3.0.CO;2-C)

41 Kim, H. M., Takadama, H., Miyaji, F., Kokubo, T., Nishiguchi, S. & Nakamura, T. 2000 Formation of bioactive functionally graded structure on Ti–6Al–4V alloy by chemical surface treatment. *J. Mater. Sci., Mater. Med.* **11**, 555–559. (doi:10.1023/A:1008924102096)

42 Kim, H. M., Takadama, H., Kokubo, T., Nishiguchi, S. & Nakamura, T. 2000 Formation of a bioactive graded surface structure on Ti–15Mo–5Zr–3Al alloy by chemical treatments. *Biomaterials* **21**, 353–358. (doi:10.1016/S0142-9612(99)00190-8)

43 Takemoto, M., Fujibayashi, S., Neo, M., So, K., Akiyama, N., Matsushita, T., Kokubo, T. & Nakamura, T. 2007 A porous bioactive titanium implant for spinal interbody fusion: an experimental study using a canine model. *J. Neurosurg. Spine* **7**, 435–443. (doi:10.3171/SPI-07/10/435)

44 Yamaguchi, S., Takadama, H., Matsushita, T., Nakamura, T. & Kokubo, T. 2010 Apatite-forming ability of Ti–15Zr–4Nb–4Ta alloy induced by calcium solution treatment. *J. Mater. Sci., Mater. Med.* **21**, 439–444. (doi:10.1007/s10856-009-3904-0)

45 Kizuki, T., Takadama, H., Matsushita, T., Nakamura, T. & Kokubo, T. 2010 Preparation of bioactive Ti metal surface enriched with calcium ions by chemical treatment. *Acta Biomater.* **6**, 2836–2842. (doi:10.1016/j.actbio.2010.01.007)

46 Fukuda, A. *et al.* 2011 Bone bonding bioactivity of Ti metal and Ti–Zr–Nb–Ta alloys with Ca ions incorporated on their surfaces by simple chemical and heat treatment. *Acta Biomater.* **7**, 1379–1386. (doi:10.1016/j.actbio.2010.09.026)

47 Pattanayak, D. K., Fukuda, A., Matsushita, T., Takemoto, M., Fujibayashi, S., Sasaki, K., Nishida, N., Nakamura, T. & Kokubo, T. 2011 Bioactive Ti metal analogous to human cancellous bone: fabrication by selective laser melting and chemical treatments. *Acta Biomater.* **7**, 1398–1406. (doi:10.1016/j.actbio.2010.09.034)

Acta Biomaterialia 7 (2011) 1398–1406

Contents lists available at ScienceDirect

Acta Biomaterialia

journal homepage: www.elsevier.com/locate/actabiomat

Bioactive Ti metal analogous to human cancellous bone: Fabrication by selective laser melting and chemical treatments

Deepak K. Pattanayak [a,*,1], A. Fukuda [b,1], T. Matsushita [a], M. Takemoto [b], S. Fujibayashi [b], K. Sasaki [c], N. Nishida [c], T. Nakamura [b], T. Kokubo [a]

[a] Department of Biomedical Sciences, College of Life and Health Sciences, Chubu University, Japan
[b] Department of Orthopaedic Surgery, Graduate School of Medicine, Kyoto University, Japan
[c] Sagawa Printing Co. Ltd., Kyoto, Japan

ARTICLE INFO

Article history:
Received 10 August 2010
Received in revised form 22 September 2010
Accepted 24 September 2010
Available online 29 September 2010

Keywords:
Selective laser melting
Porous titanium
Chemical treatment
Compressive strength
In vitro and in vivo studies

ABSTRACT

Selective laser melting (SLM) is a useful technique for preparing three-dimensional porous bodies with complicated internal structures directly from titanium (Ti) powders without any intermediate processing steps, with the products being expected to be useful as a bone substitute. In this study the necessary SLM processing conditions to obtain a dense product, such as the laser power, scanning speed, and hatching pattern, were investigated using a Ti powder of less than 45 μm particle size. The results show that a fully dense plate thinner than 1.8 mm was obtained when the laser power to scanning speed ratio was greater than 0.5 and the hatch spacing was less than the laser diameter, with a 30 μm thick powder layer. Porous Ti metals with structures analogous to human cancellous bone were fabricated and the compressive strength measured. The compressive strength was in the range 35–120 MPa when the porosity was in the range 75–55%. Porous Ti metals fabricated by SLM were heat-treated at 1300 °C for 1 h in an argon gas atmosphere to smooth the surface. Such prepared specimens were subjected to NaOH, HCl, and heat treatment to provide bioactivity. Field emission scanning electron micrographs showed that fine networks of titanium oxide were formed over the whole surface of the porous body. These treated porous bodies formed bone-like apatite on their surfaces in a simulated body fluid within 3 days. In vivo studies showed that new bone penetrated into the pores and directly bonded to the walls within 12 weeks after implantation into the femur of Japanese white rabbits. The percentage bone affinity indices of the chemical- and heat-treated porous bodies were significantly higher than that of untreated implants.

1. Introduction

Titanium (Ti) metal and its alloys are widely used for various implants in the orthopedic and dental fields, because of their good biocompatibility and high mechanical strength. However, their elastic moduli are higher than that of living bone and, hence, they are liable to induce bone resorption due to stress shielding. If a considerable amount of interconnected pores are introduced into them, their elastic moduli decrease to the level of cancellous bone. In addition, bone tissue can grow into the pores to integrate with them. Therefore, various methods have been developed for producing porous bodies of Ti metal and its alloys [1]. Among them, the most common method is sintering of metal powders with added volatile materials [2,3]. Recently, selective laser sintering (SLS) [4–10], selective laser melting (SLM) or direct laser forming (DLF) [11–18] and selective electron beam melting (SEBM) [19] processes have been applied to produce porous bone substitutes. The SLS process produces a porous body by partial sintering of metal powders. On the other hand, in the DLF/SLM and SEBM processes the metal powders are completely melted and fused by a laser or electron beam, respectively, resulting in a porous body within a short period of time [13,19]. Attempts have been made to produce various kinds of porous Ti metal with simple interconnected porous structures by the SLM process [11,12,17]. However, preparation of porous Ti metal with a structure analogous to human cancellous bone has not been reported.

In the SLM process three-dimensional (3D) structures can be prepared from metal powders without any additional processing steps. However, in order to obtain a defect-free specimen, it is essential to optimize the processing parameters of the SLM technique, i.e. laser power, scanning speed, hatching pattern, etc.

Although Ti metal and titanium alloys are biocompatible, they do not bond to living bone directly when implanted into a bone defect [20]. However, Ti metal subjected to NaOH and heat treatments to form sodium titanate on its surface spontaneously bonds

* Corresponding author. Tel.: +81 568 51 9731; fax: +81 568 51 5370.
E-mail addresses: deepak@isc.chubu.ac.jp, deepak_pattanayak@rediffmail.com (D.K. Pattanayak).
[1] The first two authors contributed equally to this study.

1742-7061/$ - see front matter © 2010 Acta Materialia Inc. Published by Elsevier Ltd. All rights reserved.
doi:10.1016/j.actbio.2010.09.034

Table 1
Chemical composition of the titanium powder (mass%).

O	Fe	H	C	N	Ni	Cr	Si	Ti
0.121	0.029	0.005	0.010	0.006	0.003	0.003	0.001	Balance

to living bone through an apatite layer formed on its surface in the living body [21–23]. This bioactive Ti metal has been applied to an artificial hip joint, and its effectiveness has already been confirmed in clinical trials [24]. This bioactive artificial hip joint (AHFIX, Japan Medical Materials Co., Japan) has been approved for clinical use in Japan since 2007.

Ti metal subjected to NaOH, HCl, and heat treatments to form Na-free titanium oxide on its surface has also been found to form a bone-like apatite layer in a simulated body fluid (SBF) [25] and to exhibit osteoconductivity as well as osteoinductivity [26–28].

In the present study plate specimens were first fabricated by the SLM process using commercially pure Ti powders. The effect of processing parameters such as power, scanning speed, and scanning pattern of the laser beam on the density of the plate specimens was investigated. Porous Ti metal with a structure analogous to human cancellous bone was prepared using the optimum operating conditions and its compressive strength measured. It was subjected to NaOH, HCl, and heat treatment for bioactivation and its apatite-forming ability in SBF and bone-bonding abilities in rabbit femurs examined.

2. Materials and methods

2.1. Materials

A gas atomized commercially pure Ti metal powder (grade 2, Osaka Titanium Technologies Co. Ltd., Japan) with a particle size of <45 μm was used as the starting powder. Its chemical composition is given in Table 1.

2.2. Selective laser melting

2.2.1. Determination of optimum conditions

Fig. 1 shows schematically the selective laser melting process. In the present experiment an SLM system (EOSINT-M270, Electro Optical Systems GmbH, Germany) was used. A 3D model was designed by computer-aided design (CAD) software (Magics, Materialise, Belgium). This 3D model was horizontally sliced into many thin layers of two-dimensional images. In this system a Yb fiber laser beam of nominal diameter 100 μm and with a maximum power of 200 W moves at a maximum speed of 7000 mm s^{-1} in an argon gas environment. According to the data for the slices provided by the computer the laser beam scans the Ti metal powder layer to selectively melt it, producing the prescribed two-dimensional metallic structures. In the next step the platform moves vertically downwards, allowing the deposition of an unfused powder layer at a 30 μm interval. Again, the laser beam selectively melts the second layer over the first layer, and this process is continued repeatedly to construct the final 3D metallic structure. The manufactured specimen was removed from the platform. The specimens were cleaned ultrasonically using acetone, 2-propanol, and ultrapure water for 30 min each to remove residual unfused powder sticking to the walls of the specimen.

Fig. 2 shows the standard scanning strategy for the fabrication of the specimen using a boundary contour beam of 58.5 W power followed by a hatch beam of 117 W, with a hatch space of 180 μm and a hatch offset of 20 μm. In each subsequent layer the hatch lines are rotated with respect to the previous layer by 66.7° to melt the powder completely. In order to investigate the effect of energy density on the density of the fabricated specimen, the laser power was varied from 90 to 180 W at a constant scanning speed of 225 mm s^{-1} and constant powder layer of 30 μm thickness, so that the power to speed ratio (P/V) was in the range 0.3–0.8 W mm^{-1} s^{-1}. Specimens of $9 \times 9 \times 9$ mm^3 size were formed at different P/V ratios. Their densities were measured using Archimedes' principle. In addition to the above, $9 \times 9 \times t$ mm^3 specimens of different thicknesses (t) were formed by using a hatch space of 90 and 180 μm, and their densities were also measured using the same technique.

2.2.2. Fabrication of a porous structure analogous to human cancellous bone

Porous Ti metals with a structure similar to that of human cancellous bone with different porosities were fabricated using the optimized processing conditions of laser power, scanning speed, and hatching pattern. In this process micro-CT images of the structure of cancellous bone were stored in a computer and modified a little due to certain limitations of this method. For example, wall thicknesses of less than 200 μm are difficult to process and, hence, the wall thickness was increased to more than 300 μm. In this process specimens were always prepared from the bottom to the top.

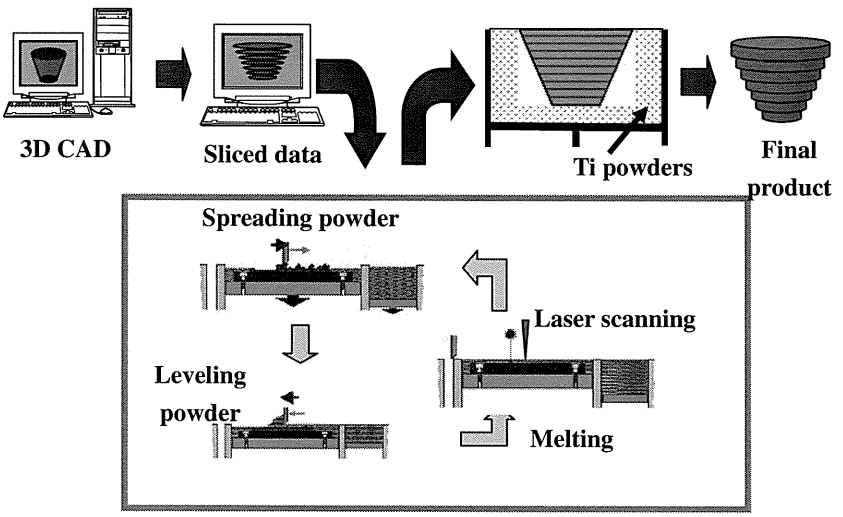

Fig. 1. Schematic representation of the SLM process.

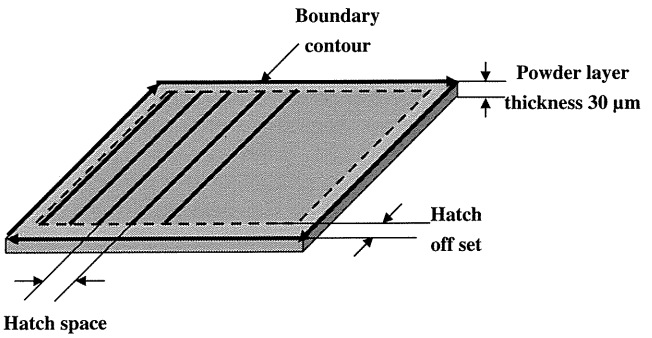

Fig. 2. Schematic representation of various operating parameters which affect the product density in the SLM process.

Therefore, a foothold was provided for the bone structure. Then the image was sliced at 30 μm intervals. Porous structures were fabricated using Ti metal powder according to the sliced data by the method described in Section 2.2.1. Fig. 3a shows a CT image of the cancellous bone structure of a 53-year-old male, while (i) is a porous body produced by multiple stacking of the unit structure in (a). Fig. 3b shows a CT image of the cancellous bone of a 48-year-old female, while (ii) is a porous body produced from (b). Fig. 3ii is referred to as CBS in subsequent studies. Fig. 3c shows a hollow cubic unit cell and its stacking, while (iii) is a porous body produced from (c). This is referred to as IPS in subsequent studies. These three types of specimens were produced with different porosities by changing the wall thickness. Cancellous bone structures consist of interconnected pores of different sizes ranging from 500 μm to 2 mm (Fig. 3i and ii), while the cubic structure has interconnected pores in the range 400–800 μm (Fig. 3iii). These specimens were washed with acetone, 2-propanol, and ultrapure water for 30 min each in an ultrasonic cleaner and then dried in an oven at 40 °C overnight. Later, the CBS and IPS specimens were subjected to heat treatment at 1300 °C in an argon gas atmosphere to smooth the surface.

2.3. Chemical and heat treatment for bioactivity

The porous Ti metal specimens CBS and IPS were first soaked in 5 M NaOH solution at 60 °C for 24 h and then soaked in 0.5 mM HCl solution at 40 °C for 3 h to bioactivate them. A continuous-flow method was used to treat these specimens to avoid non-uniform chemical treatment inside the pores along the length. Later, these specimens were washed in ultrapure water, dried in an oven at 40 °C overnight and then heated to 600 °C at a rate of 5 °C min^{-1}. The specimens were kept in a Fe–Cr electric furnace under an air atmosphere at 600 °C for 1 h and finally cooled to room temperature naturally in the furnace.

2.4. Analysis of the surface structures and measurement of compressive strength

The surface texture of the porous Ti metal as prepared, in addition to being subsequently subjected to heat treatment at 1300 °C in an argon gas atmosphere, was observed by field emission scanning electron microscopy (FE-SEM) (Hitachi S-4300, Japan). Surface structural changes due to the NaOH, HCl, and heat treatments and subsequent soaking in SBF were also observed by FE-SEM.

The compressive strengths of porous bodies of Ti metal with the different structures shown in Fig. 3i–iii were measured using a universal testing machine (model EHF-LV020K1-010, Shimadzu Corp., Japan) at a cross-head speed of 1 mm min^{-1}.

2.5. Examination of the apatite forming ability in a simulated body fluid (SBF)

Porous Ti metal subjected to chemical and heat treatment was soaked in 30 ml of an acellular SBF with ion concentrations of Na^+ 142.0, K^+ 5.0, Mg^{2+} 1.5, Ca^{2+} 2.5, Cl^-147.8, HCO_3^- 4.2, HPO_4^{2-} 1.0, and SO_4^{2-} 0.5 mM, nearly equal to those of human blood plasma, at 36.5 °C for 3 days. The SBF was prepared by dissolving reagent grade NaCl, $NaHCO_3$, KCl, $K_2HPO_4{\cdot}3H_2O$, $MgCl_2{\cdot}6H_2O$, $CaCl_2$, and Na_2SO_4 (Nacalai Tesque Inc., Kyoto, Japan) in ultrapure

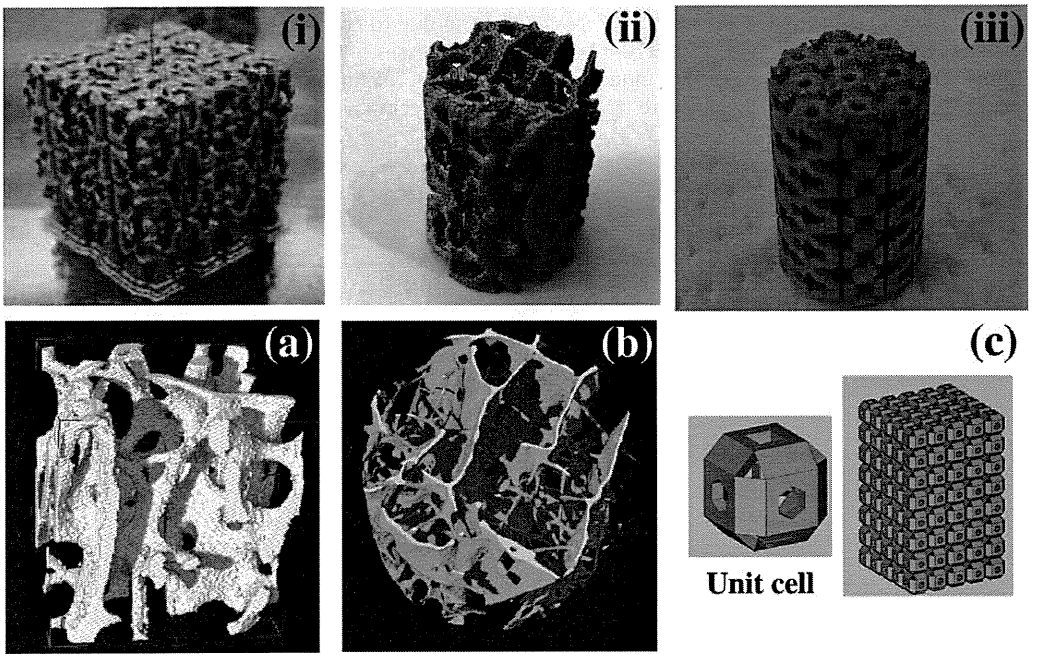

Fig. 3. Titanium porous structure fabricated by SLM (i–iii) based on micro-CT images of human cancellous bones (a, b) and stacked hollow cubes (c). Specimen size: (a) 15 × 15 × 15 mm; (b, c) 6 mm diameter, 10 mm length. Notation: (ii) CBS; (iii) IPS.

water buffered at pH 7.40 with Tris and 1 M HCl (Nacalai Tesque) [29]. After 3 days soaking the specimens were removed from the SBF, gently washed with ultrapure water, and dried at 40 °C in an oven. Apatite formation on the walls was examined by FE-SEM.

2.6. In vivo examination of new bone formation in white rabbits

2.6.1. Animal study

Porous Ti metal specimens of CBS and IPS 6 mm in outer diameter and 15 mm in length, subjected to chemical and heat treatments, were conventionally sterilized using ethylene oxide gas and implanted into the metaphyses of the femoral condyles of mature male Japanese white rabbits weighing 2.8–3.5 kg. The surgical methods used have been described elsewhere [30,31]. Briefly, the rabbits were anesthetized with intravenous injections of sodium pentobarbital (0.5 ml kg^{-1}), an intramuscular injection of ketamine hydrochloride (10 mg kg^{-1}), and local administration of a solution of 1% lidocaine. After shaving, disinfection, and draping, the fascia was split and a 6 mm diameter drill hole was made through the femoral condyles. After irrigating the hole with saline, both kinds of porous Ti metal specimens, CBS and IPS, subjected to chemical and heat treatment, were implanted into the hole. For comparison, untreated samples were also implanted in a similar manner. Surgical procedures were performed bilaterally. Twenty-five rabbits were used for the chemical- and heat-treated implants. At 3, 6, 12, 26, and 52 weeks after implantation five rabbits were killed using an overdose of intravenous sodium pentobarbital, i.e. five chemical- and heat-treated implants and five animals per experimental condition. Ten rabbits were used for the untreated implants. At 12 and 52 weeks after implantation these rabbits were killed in the same way, i.e. five untreated implants and five animals per experimental condition. This animal study was approved by the Animal Research Committee, Graduate School of Medicine, Kyoto University, Japan.

2.6.2. Histological examination

Following death the implant sites were removed and prepared for histology. The specimens were fixed in 10% phosphate-buffered formalin, pH 7.25 for 7 days and dehydrated in serial concentrations of ethanol (70%, 80%, 90%, 99%, 100%, and 100% v/v) for 3 days each. Specimens were then embedded in polyester resin. Thick sections (250 μm) were cut with a band saw (BS-3000CP, EXACT Cutting Systems, Norderstedt, Germany) perpendicular to the axis of the implant and ground to a thickness of 50–60 μm using a grinding–sliding machine (Microgrinding MG-4000, EXACT Cutting Systems). Each section was then stained with Stevenel's blue and Van Gieson's picrofuchsin [32]. A thorough microscopic analysis was performed on histological slides using transmitted light microscopy (model Eclipse 80i, Nikon Co., Japan) combined with a digital camera (model DS-5 M-L1, Nikon Co., Japan).

Other thick sections (500 μm) were cut with a band saw, polished with diamond paper, and a thin layer of carbon applied for observation by SEM.

2.6.3. Histomorphometric examination

The bone affinity index (%) was measured on a personal computer using Adobe Photoshop CS3 and Image J (NIH) for each implant using data provided by light microscopy and fluorescence microscopy. The bone affinity index is defined as the fraction of bone contact over the entire wall of the pores in the implant [26,31,33]. Two sections surrounded with cancellous bone from either the medial or the lateral condyles were examined for each implant. Thus, 10 slices were analyzed for each implantation time.

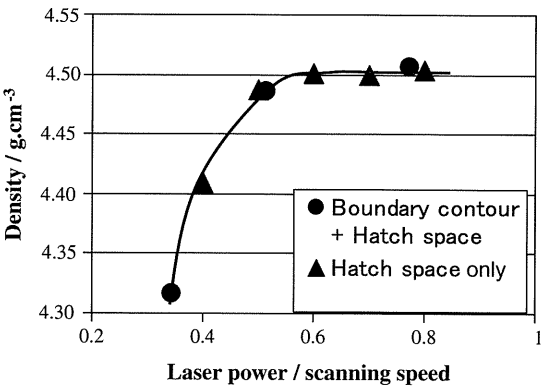

Fig. 4. Variation in density of the solid cubic specimens with change in laser power to scanning speed ratio at a constant powder layer thickness. Specimen size 9 × 9 × 9 mm^3; hatch space 180 μm; scanning speed 225 mm s^{-1}.

2.6.4. Statistical analysis

All data are expressed as means ± standard deviation (SD) and were statistically analyzed using JMP IN 5.1 (SAS Institute, Cary, NC). The unpaired one-tailed Student's *t*-test was used for comparison between the implant (bioactive treated and untreated) at each time point (12 and 52 weeks). One-way ANOVA followed by post hoc tests (Tukey–Kramer multiple comparison tests) were used to analyze temporal bone formation in each implant type. Differences at $P < 0.05$ were considered statistically significant.

3. Results

3.1. Effects of processing parameters on the density of the specimen

Fig. 4 shows the variation in density of specimens with laser power to scanning speed (*P*/*V*) ratio, where specimens were fabricated using a boundary contour followed by a hatch beam with a hatch space of 180 μm. Specimens were also prepared using only a hatch beam with a hatch space of 180 μm. From Fig. 4 we can see that in both cases the density of the specimen was low when the *P*/*V* ratio was <0.5, and reached the theoretical density (4.51 g cm^{-3}) of Ti metal when the P/V ratio was >0.60.

Fig. 5 shows the density of Ti plates of different thicknesses, which were fabricated at two different hatch beam spaces of 90 and 180 μm at a constant *P*/*V* ratio of 0.51. The density was nearly equal to that of the theoretical density when the thickness of the prepared specimen was >1.8 mm, irrespective of the space between the two consecutive hatch beams. A high density was observed for plates with a thickness of <1.8 mm when the hatch beam space was 90 μm. The effect of hatch beam offsets of 0, 10,

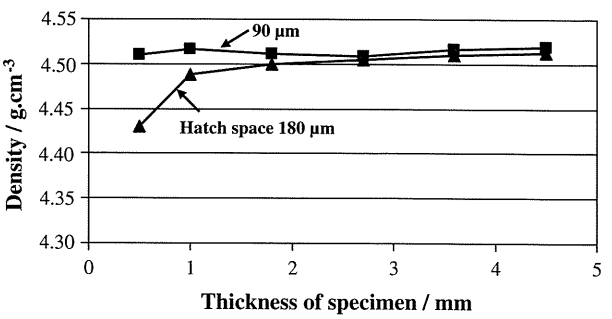

Fig. 5. Effect of hatch space on density of solid specimens of different thicknesses. Specimen size 9 × 9 × *t* mm^3, where *t* is the thickness of specimen in mm; scanning speed 225 mm s^{-1}.

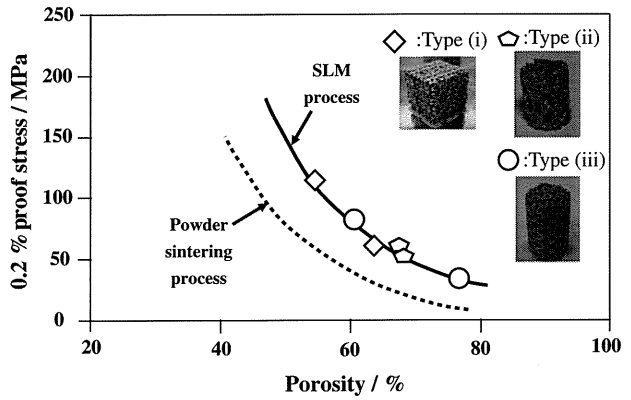

Fig. 6. Compressive strength of porous Ti metal with respect to porosity prepared by selective laser melting and compared with those prepared by a conventional powder sintering process.

and 20 μm on the density of the specimens was also examined, and the results showed similar densities of the final products in all cases.

Based on these results, a laser power of 117 W, scanning speed of 225 mm s^{-1}, hatch space of 90 μm, and hatch offset of 20 μm were used to fabricate porous bodies with a wall thickness of <1.8 mm.

3.2. Compressive strength of the porous specimens

The wall thicknesses of the various types of fabricated porous structures shown in Fig. 3 were in the range 400–800 μm. Cancellous bone structures consist of pores of different sizes ranging from 500 μm to 2 mm (Fig. 3i and ii), while the cubic structure has pores in the range 400–800 μm (Fig. 3iii). The compressive strengths of the various kinds of porous Ti metal fabricated by the SLM process is plotted against porosity in Fig. 6. The compressive strength was in the range 35–120 MPa when the porosities were in the range 75–55%. The results were compared with those of porous Ti metal prepared by the powder sintering method. The compressive strength of porous specimens fabricated by SLM was higher than that of those prepared by powder sintering, while the strength of specimens generated by both methods decreased with increasing porosity [3].

3.3. Surface structural changes on heat treatment

Fig. 7 shows the surface texture of the fabricated specimen, as well as of that subjected to heat treatment at 1300 °C in an argon gas atmosphere. Partially melted Ti particles were loosely bonded to the surface of the fabricated specimen. However, after heat treatment at 1300 °C, these particles were fused and bonded with the laser melted core part, producing a concave texture over the entire surface.

3.4. Surface structural changes in porous Ti metal on chemical and heat treatment and soaking in SBF

Fig. 8 shows FE-SEM photographs of a porous Ti metal that had been subjected to chemical and heat treatment after heat treatment at 1300 °C in an argon gas atmosphere. A fine network structure was formed on the surface of the porous Ti metal. These network structures were uniformly observed, even on the inner side of the pore.

Fig. 9 shows FE-SEM photographs of porous Ti metal soaked in SBF for 3 days after chemical and heat treatment. The walls of the porous body were completely covered with apatite after soaking in SBF for 3 days, indicating that the Ti metal surface had become bioactive after NaOH, HCl, and heat treatment.

3.5. In vivo bioactivity of the porous Ti metal

Gross inspection of the animal experiments showed that all rabbits tolerated the operative procedure well. No infection of the

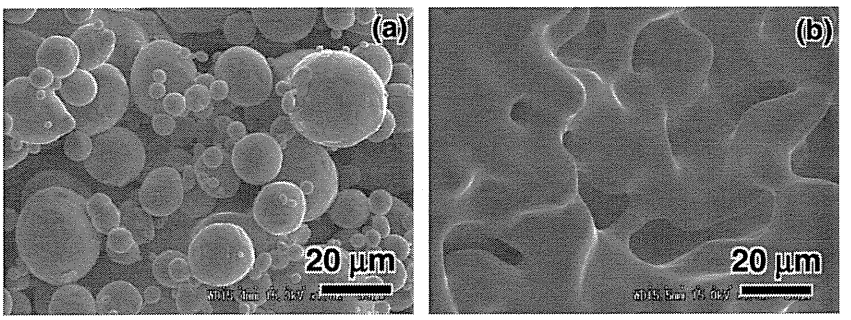

Fig. 7. FE-SEM photograph of the surface of porous Ti metal CBS (a) fabricated by SLM and (b) that heated at 1300 °C for 1 h in an argon gas atmosphere.

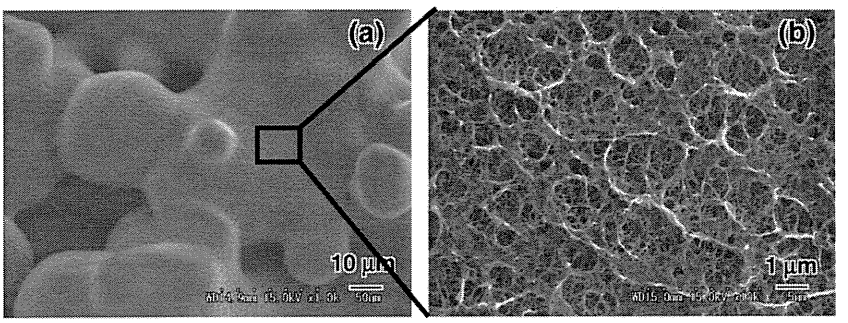

Fig. 8. FE-SEM photograph of porous Ti metal CBS subjected to NaOH, HCl and heat treatments after heat treatment at 1300 °C. (a) Low magnification; (b) high magnification showing fine network structure on the wall.

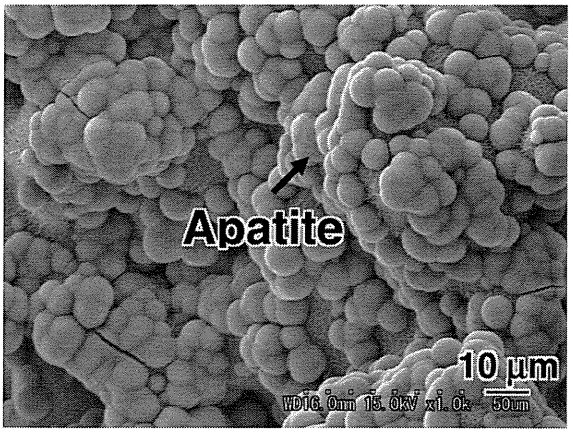

Fig. 9. Apatite particles formed on the surface of porous Ti metal CBS soaked in SBF for 3 days after NaOH, HCl and heat treatments.

operative site or dislocations of the implants were observed on dissection after death. All implanted porous Ti metal CBS and IPS specimens were stable and firmly bonded with the host bone at all post-implantation time points. No apparent adverse reactions, such as inflammation or foreign body reactions, were noted on or around any implanted samples by Stevenel's blue and Van Gieson's surface staining.

Within 3 weeks new bone was observed at the outer periphery and in the center of the chemical- and heat-treated specimens (results not shown). At the advancing bone front in the deep portion of the sample immature woven bone was found. There was no sign of cartilage formation or endochondral ossification. Marrow-like tissue formation was observed in the samples. Fig. 10 shows light microscope and SEM photographs of chemical- and heat-treated and untreated CBS samples 12 weeks after implantation. From Fig. 10 we can see that new bone was formed on the porous surface and bonded directly with the chemically treated layer. On the other hand, little new bone formation was observed on the surface of untreated implants. Fig. 11 shows a comparative histological study of porous Ti metal CBS and IPS samples subjected to chemical and heat treatment and implanted into the femurs of rabbits for 12 weeks. From Fig. 11 we can see that both CBS and IPS specimens showed mature bone strongly adhering to the porous wall. Fig. 12 shows the bone affinity indices (%) for chemical- and heat-treated CBS and IPS samples as well as for untreated samples for different implantation periods. The affinity indices of chemical- and heat-treated porous Ti metal CBS and IPS samples gradually increased with implantation period. There was a significant difference between the 52 week period and the other periods for the chemical- and heat-treated porous Ti metal CBS and IPS samples. After 12 and 52 weeks implantation the affinity indices of chemical- and heat-treated implants were significantly greater than those of the untreated implants.

4. Discussion

Using conventional fabrication techniques it is difficult to control the internal pore geometry, pore size, and distribution [3,34]. On the other hand, the SLM process is a useful technique to fabricate 3D porous structures directly from metallic powders and, hence, the process is suitable for the design of artificial bone substitutes with complex inner and outer geometries fitting the patient's defective bone. However, in this technique fine metal powders are melted by laser beam, which moves at a very high speed, and hence, this melting process may create internal defects due to some of the powder being blown off. In order to fabricate defect-free metallic implants it is important to optimize the power, scanning speed, and scanning pattern of the laser beam.

When the supplied energy density is insufficient to fully melt the powder, unmelted powder remains on the layer and produces defects. The temperature of the powder in the vicinity of the melted zone is low. In contrast, when the supplied energy density is sufficient to melt the powder, the melting zone becomes large and the temperature in the vicinity of the melted zone will remain high. This high temperature assists full melting of the powder in the next layer. Therefore, the density of the specimen depends

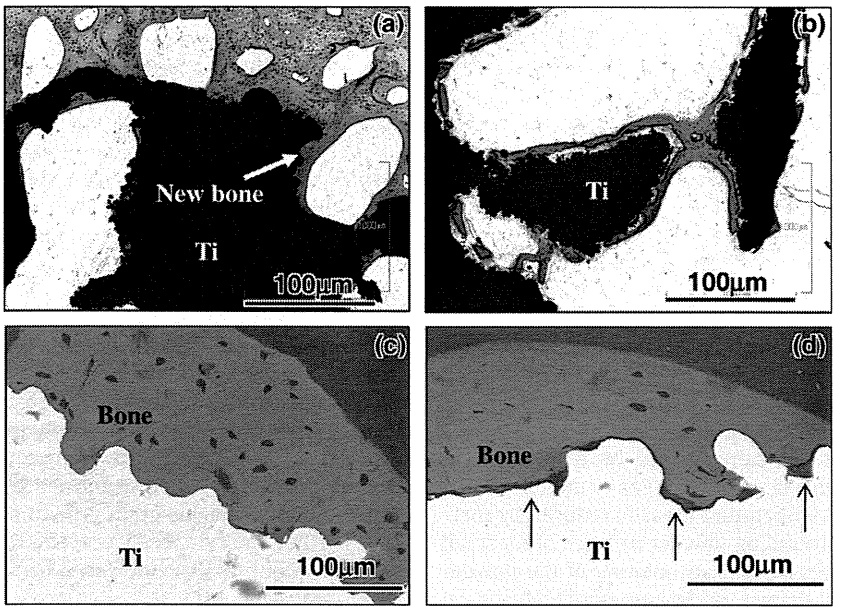

Fig. 10. Stevenel's blue and Van Gieson's surface staining of non-decalcified histological sections and SEM photographs of CBS samples after 12 weeks implantation. (a, c) Chemical- and heat-treated implants show new bone formation along the pore walls; (b, d) untreated implants show slight new bone formation along the pore walls. Red indicates bone. (For interpretation of the references to colour in this figure legend, the reader is referred to the web version of this article).

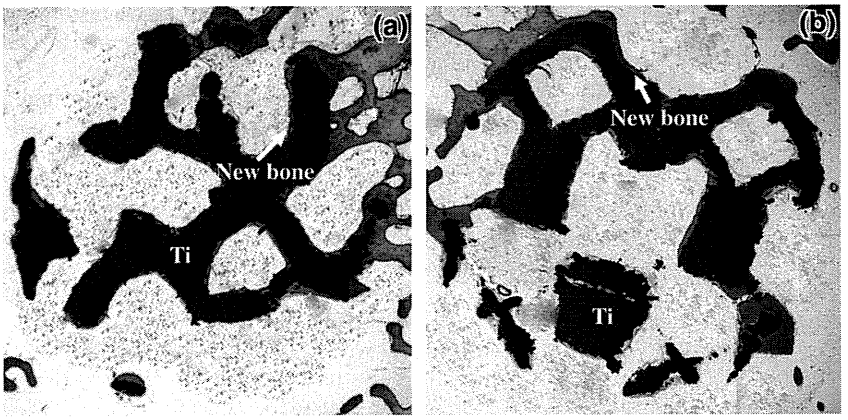

Fig. 11. Stevenel's blue and van Gieson's surface staining of non-decalcified histological section of chemical- and heat-treated porous Ti implants CBS and IPS after 12 weeks implantation in the femur of white rabbits.

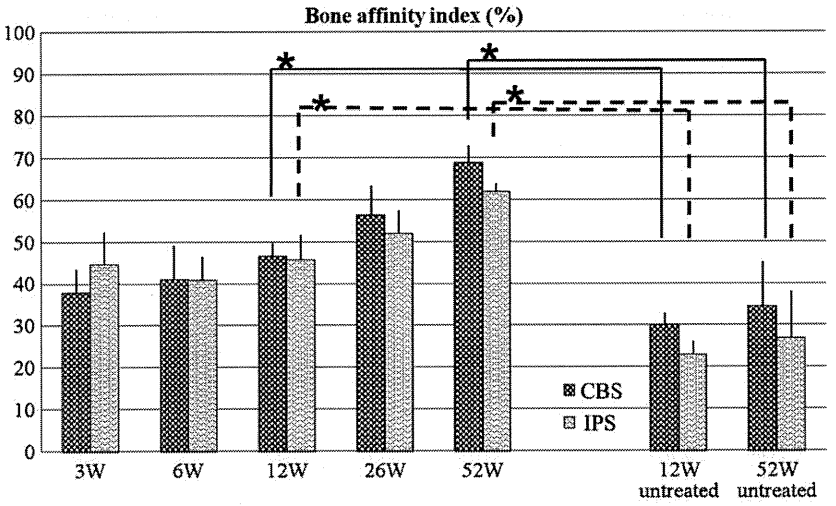

Fig. 12. Affinity indices (%) of the chemical- and heat-treated porous Ti implants CBS and IPS implanted in the femur of rabbit for different durations. The error bars are standard deviations. * Significant difference.

on the supplied energy density or on the ratio of laser power to scanning speed (P/V) at a constant thickness of powder layer. The critical value of P/V is approximately 0.5–0.6, as shown in Fig. 4. In general, both a boundary contour and a hatch beam are necessary to give an accurate shape and high density to the final product. However, similar trends in density as a function of P/V were observed when the specimens were fabricated using only a hatch beam, as shown in Fig. 4. As indicated in Fig. 5, the density of the thick plate specimen (>1.8 mm) does not depend on two consecutive hatch spaces. However, a large number of defects remained in the formed body when thin plate specimens (thinner than 1 mm) were fabricated with a hatch spacing of 180 μm, and their densities were low. A fully dense body with a thinner wall measuring 0.5 mm could be prepared by decreasing the space between the two consecutive hatch beams to 90 μm, as shown in Fig. 5. This suggests that two consecutive beams should be overlapped to fabricate thinner walls. When a laser beam scans to melt the powders to form a thin wall, the temperature is easily reduced by thermal conduction into the surrounding powder because of its small thermal capacity. This induces insufficient melting of the powder and the formation of internal defects. In the case of the fabrication of thick walls, the laser power is supplied over a wide zone, so the powder surrounding the melt zone remains hot for a longer time, which helps in melting of the Ti powder to reduce the defects and increase the density. If the hatch beam scanning interval is further reduced, defect formation can be avoided, because the energy supplied to the powder for each unit volume is sufficient to keep the temperature high in the melt zone.

In the present study we observed that large numbers of spherical Ti particles were partially bonded to the porous walls. In order to avoid release of these particles, the specimens were heated at 1300 °C in an argon gas atmosphere (Fig. 7). Although the mechanical strength might be decreased by the heat treatment [35], microcavities were formed on the wall, and these might be beneficial for interlock with the surrounding tissues when implanted in the living body. The compressive strength of the porous body processed by SLM was in the range 35–120 MPa when the volumetric porosities were in the range 75–55%. These values are higher than those of porous bodies prepared by the powder sintering method, as seen in Fig. 6. The improved compressive strength is attributed to the fine grain structure formed by rapid cooling of the laser melted body, whereas grain growth occurs during powder sintering. Further, the compressive strength of the porous body prepared by SLM might be little increased by the subsequent chemical and heat treatments [3].

Porous bodies prepared by the SLM process formed a fine uniform network structure on their pore walls after NaOH treatment, and these network structures remained stable even after subse-

quent HCl and heat treatment, as shown in Fig. 8. These network structures, as reported earlier, consist of anatase and rutile [25]. Chemical treatment has the advantage of uniform treatment, even within the pore. Porous bodies subjected to this chemical and heat treatment formed bone-like apatite on soaking in SBF within 3 days, as seen in Fig. 9. It has been believed that if a material forms a bone-like apatite layer on its surface in SBF it can induce direct bone formation through a similar apatite layer in the living body and bond to living bone [21,22]. In the present study similar results were verified in the animal experiments. As shown in Fig. 11, newly formed bone was observed on the periphery and in the center of both kinds of porous structures, CBS and IPS, within 12 weeks after implantation into the femurs of white rabbits. Porous CBS implants showed new bone formation (Fig. 10) in pores and bonded to the wall having nano-structured fine network structures due to previous NaOH, HCl, and heat treatments. On the other hand, untreated implants showed little bone formation in the pores. The amount of new bone on the surface of the untreated implants barely increased with time.

New bone on the surface of chemical- and heat-treated porous Ti metal CBS and IPS gradually increased with implantation time, compared with the untreated porous samples (Fig. 12). This indicates that the porous Ti metal fabricated by the SLM process has a high osteoconductive ability after subsequent NaOH, HCl, and heat treatments, the same as that of plasma sprayed porous Ti metal, as reported earlier [26,36]. Further detailed investigations on the influence of the porous structure on bone growth is in progress, and will be reported elsewhere.

The present study has shown that a porous structure consisting of thin-walled titanium metal with a structure similar to that of human cancellous bone could be prepared by the SLM process by optimizing the laser power, scanning speed, and hatching pattern. This SLM process could be useful to fabricate custom-made implants for biomedical applications tailored to the patient. Internal structure and porosity level can be easily controlled by the automated manufacturing process and, further, bioactivity can be provided by the subsequent chemical and heat treatments.

5. Conclusion

In order to fabricate a porous Ti metal with fully dense thin walls by a SLM process, laser power, scanning speed, and hatching pattern were optimized and various kind of porous bodies were fabricated. The compressive strength of the porous bodies prepared by SLM was found to be higher than that of a powder sintering process at the same level of porosity. Thus, the prepared porous structures analogous to human cancellous bone, when subjected to chemical and heat treatments, uniformly formed a fine network structure of titanium oxide layer, which formed bone-like apatite in SBF within 3 days. In vivo studies showed that newly formed bone was observed in the periphery and in the center of the chemical- and heat-treated cylindrical porous body within 12 weeks of implantation into the rabbit femoral condyle, and was directly bonded to the titanium wall. The SLM process has been found to be a useful technique for fabricating customized metallic implants with complicated internal structures, and the porous bodies thus fabricated are expected to be a useful bone substitutes after chemical and heat treatments.

Appendix A. Figures with essential colour discrimination

Certain figures in this article, particularly Figures 1–3, 6, 10 and 11 are difficult to interpret in black and white. The full colour images can be found in the on-line version, at doi:10.1016/j.actbio.2010.09.034.

References

[1] Ryan G, Pandit A, Apatsidis DP. Fabrication methods of porous metals for use in orthopaedic applications. Biomaterials 2006;27:2651–70.
[2] Wen CE, Yamada Y, Shimojima K, Chino Y, Hosokawa H, Mabuchi M. Novel titanium foam for bone tissue engineering. J Mater Res 2002;17:2633–9.
[3] Pattanayak DK, Matsushita T, Doi K, Takadama H, Nakamura T, Kokubo T. Effects of oxygen content of porous titanium metal on its apatite-forming ability and compressive strength. J Mater Sci Eng C 2009;29:1974–8.
[4] Das S, Wohlert M, Beaman JJ, Bourell DL. Processing of titanium net shapes by SLS/HIP. Mater Des 1999;20:115–21.
[5] Fischer P, Romano V, Weber HP, Karapatis NP, Boillat E, Glardon R. Sintering of commercially pure titanium powder with a Nd:YAG laser source. Acta Mater 2003;51:1651–62.
[6] Simchi A, Petzoldt F, Pohl H. On the development of direct metal laser sintering for rapid tooling. J. Mater Process Technol 2003;141:319–28.
[7] Williams JM et al. Bone tissue engineering using polycaprolactone scaffolds fabricated via selective laser sintering. Biomaterials 2005;26:4817–27.
[8] Santos EC, Shiomi M, Osakada K, Laoui T. Rapid manufacturing of metal components by laser forming. Int J Machine Tools Manuf 2006;46:1459–68.
[9] Traini T, Mangano C, Sammons RL, Mangano F, Macchi A, Piattelli A. Direct laser metal sintering as a new approach to fabrication of an isoelastic functionally graded material for manufacture of porous titanium dental implants. Dent Mater 2008;24:1525–33.
[10] Kumar S, Kruth JP. Composites by rapid prototyping technology. Mater Des 2010;31:850–6.
[11] Hollander DA, Walter MV, Wirtz T, Sellei R, Rohlfing BS, Paar O, et al. Structural, mechanical and in vitro characterization of individually structured Ti6Al4V produced by direct laser forming. Biomaterials 2006;27:955–63.
[12] Lin CY, Wirtz T, LaMarca F, Hollister SJ. Structural and mechanical evaluations of a topology optimized titanium interbody fusion cage fabricated by selective laser melting process. J Biomed Mater Res A 2007;83:272–9.
[13] Yadroitsev I. Bertrand Ph, Smurov I. Parametric analysis of the selective laser melting process. Appl Surf Sci 2007;253:8064–9.
[14] Mullen L, Stamp RC, Brooks WK, Jones E, Sutcliffe CJ. Selective laser melting: a regular unit cell approach for the manufacture of porous, titanium, bone ingrowth constructs, suitable for orthopedic applications. J Biomed Mater Res B Appl Biomater 2009;89:325–34.
[15] Mullen L, Stamp RC, Fox P, Jones E, Ngo C, Sutcliffe CJ. Selective laser melting: a unit cell approach for the manufacture of porous, titanium, bone in-growth constructs, suitable for orthopedic applications. II. Randomized structures. J Biomed Mater Res B Appl Biomater 2009;92:178–88.
[16] Hao L, Dadbakhsh S, Seaman O, Felstead M. Selective laser melting of a stainless steel and hydroxyapatite composite for load-bearing implant development. J Mater Process Technol 2009;209:5793–801.
[17] Stamp R, Fox P, Neill WO, Jones E, Sutcliffe C. The development of a scanning strategy for the manufacture of porous biomaterials by selective laser melting. J Mater Sci Mater Med 2009;20:1839–48.
[18] Thijs L, Verhaeghe F, Craeghs T, Humbeeck JV, Kruth JP. A study of the microstructural evolution during selective laser melting of Ti6Al4V. Acta Mater 2010;58:3303–12.
[19] Heinl P, Muller L, Korner C, Singer RF, Muller FA. Cellular Ti–6Al–4V structures with interconnected macro porosity for bone implants fabricated by selective electron beam melting. Acta Biomater 2008;4:1536–44.
[20] Hacking SA, Tanzer M, Harvey EJ, Krygier JJ, Bobyn JD. Relative contributions of chemistry and topography to the osseointegration of hydroxyapatite coatings. Clin Orthoped Rel Res 2002;405:24–38.
[21] Kim HM, Miyaji F, Kokubo T, Nakamura T. Preparation of bioactive Ti and its alloys via simple chemical surface treatment. J Biomed Mater Res 1996;32:409–17.
[22] Nishiguchi S, Fujibayashi S, Kim HM, Kokubo T, Nakamura T. Biology of alkali- and heat-treated titanium implants. J Biomed Mater Res A 2003;67:26–35.
[23] Fujibayashi S, Neo M, Kim HM, Kokubo T, Nakamura T. Osteoinduction of porous bioactive titanium metal. Biomaterials 2004;25:443–50.
[24] Kawanabe K et al. A new cementless total hip arthroplasty with bioactive titanium porous coating by alkaline and heat treatment: average 4.8 year results. J Biomed Mater Res B Appl Biomater 2009;90:476–81.
[25] Pattanayak DK, Kawai T, Matsushita T, Takadama H, Nakamura T, Kokubo T. Effect of HCl concentrations on apatite-forming ability of NaOH–HCl- and heat-treated titanium metal. J Mater Sci Mater Med 2009;20:1401–11.
[26] Takemoto M, Fujibayashi S, Neo M, Suzuki J, Kokubo T, Nakamura T. Mechanical properties and osteoconductivity of porous bioactive titanium. Biomaterials 2005;26:6014–23.
[27] Takemoto M, Fujibayashi S, Neo M, Suzuki J, Matsushita T, Kokubo T, et al. Osteoinductive porous titanium implants: effect of sodium removal by dilute HCl treatment. Biomaterials 2006;27:2682–91.
[28] Takemoto M et al. A porous bioactive titanium implant for spinal interbody fusion: an experimental study using a canine model. J Neurosur Spine 2007;7:435–43.
[29] Kokubo T, Takadama H. How useful is SBF in predicting in vivo bone bioactivity? Biomaterials 2006;27:2907–15.

[30] Fujibayashi S, Nakamura T, Nishiguchi S, Tamura J, Uchida M, Kim HM, et al. Bioactive titanium: effect of sodium removal on the bone-bonding ability of bioactive titanium prepared by alkali and heat treatment. J Biomed Mater Res 2001;56:562–70.
[31] Fujibayashi S, Neo M, Kim HM, Kokubo T, Nakamura T. A comparative study between in vivo bone ingrowth and in vitro apatite formation on Na_2O–CaO–SiO_2 glasses. Biomaterials 2003;24:1349–56.
[32] Maniatopoulos C, Rodriguez A, Deporter DA, Melcher AH. An improved method for preparing histological sections of metallic implants. Int J Oral Maxillofac Implants 1986;1:31–7.
[33] Nakamura T, Takemoto M. Osteoconduction and its evaluation. In: Kokubo T, editor. Bioceramics and their clinical applications. Cambridge: Woodhead Publishing; 2008. p. 183–98.
[34] Yang YZ, Tian JM, Tian JT, Chen ZQ, Deng XJ, Zhang DH. Preparation of graded porous titanium coatings on titanium implant materials by plasma spraying. J Biomed Mater Res 2000;52:333–7.
[35] Pattanayak DK et al. Fabrication of bioactive porous Ti metal with structure similar to human cancellous bone by selective laser melting. Bioceramics 2009;22:163–6.
[36] Tanaka K, Takemoto M, Fujibayashi S, Kawanabe K, Matsushita T, Kokubo T, et al. Long-term study of osteoconductivity of bioactive porous titanium metals: effect of sodium removal by dilute HCl treatment. Key Eng Mater 2009;396–398:353–6.

Eur Spine J
DOI 10.1007/s00586-011-1728-3

ORIGINAL ARTICLE

A novel synthetic material for spinal fusion: a prospective clinical trial of porous bioactive titanium metal for lumbar interbody fusion

Shunsuke Fujibayashi · Mitsuru Takemoto · Masashi Neo · Tomiharu Matsushita · Tadashi Kokubo · Kenji Doi · Tatsuya Ito · Akira Shimizu · Takashi Nakamura

Received: 6 December 2010 / Revised: 23 January 2011 / Accepted: 16 February 2011

Abstract The objective of this study was to establish the efficacy and safety of porous bioactive titanium metal for use in a spinal fusion device, based on a prospective human clinical trial. A high-strength spinal interbody fusion device was manufactured from porous titanium metal. A bioactive surface was produced by simple chemical and thermal treatment. Five patients with unstable lumbar spine disease were treated surgically using this device in a clinical trial approved by our Ethics Review Committee and the University Hospital Medical Information Network. Clinical and radiological results were reported at the minimum follow-up period of 1 year. The optimal mechanical strength and interconnected structure of the porous titanium metal were adjusted for the device. The whole surface of porous titanium metal was treated uniformly and its bioactive ability was confirmed before clinical use. Successful bony union was achieved in all cases within 6 months without the need for autologous iliac crest bone grafting. Two specific findings including an anchoring effect and gap filling were evident radiologically. All clinical parameters improved significantly after the operation and no adverse effects were encountered during the follow-up period. Although a larger and longer-term follow-up clinical study is mandatory to reach any firm conclusions, the study results show that this porous bioactive titanium metal is promising material for a spinal fusion device.

Keywords Porous titanium metal · Spinal fusion · Biomaterial · Clinical trial

S. Fujibayashi (✉) · M. Takemoto · M. Neo · T. Nakamura
Department of Orthopedic Surgery,
Graduate School of Medicine, Kyoto University,
Kyoto 606-8507, Japan
e-mail: shfuji@kuhp.kyoto-u.ac.jp

T. Matsushita · T. Kokubo
Department of Biomedical Sciences, College of Life and Health Sciences, Chubu University, Kasugai 487-8501, Japan

K. Doi
Osaka Yakin Kogyou Co.,Ltd, Miki 673-0043, Japan

T. Ito · A. Shimizu
Department of Experimental Therapeutics,
Translational Research Center,
Kyoto University Hospital, Kyoto 606-8507, Japan

Introduction

Osteoconductive synthetic materials including sintered hydroxyapatite ($Ca_{10}(PO_4)_6(OH)_2$ or HA), Na_2O-CaO-SiO_2-P_2O_5 system (Bioglass®) and glass ceramics containing apatite and wollastonite (AW-GC) are widely used clinically as bone substitutes [7, 12, 16]. Because application for load-bearing conditions such as the spine or long bones requires high mechanical strength, solid materials are usually used. However, such materials are brittle against shearing forces and bond to the surrounding bone only at their surface. Porous materials have advantages over solid materials in terms of bone bonding, because they can demonstrate both osteoconductive bonding and mechanical interlocking through bone tissue ingrowth into the pores. Conventional porous synthetic materials such as granules of HA and AW-GC have been applied clinically as bone graft expanders for lumbar posterolateral fusion or bone void fillers after tumor excision [8]. However, because of their poor mechanical strength, porous body of such materials cannot be applied in load-bearing conditions. Thus, achieving both high bone-bonding ability and high mechanical strength is quite difficult for porous

Published online: 03 March 2011

materials. To overcome this problem, we have developed porous bioactive titanium metal, which possesses both high bone-bonding ability and high mechanical strength simultaneously [24]. Titanium metal and its alloys can be changed to bioactive materials by simple chemical and thermal surface treatment [9, 18]. This can be applied to porous titanium metal as well [15]. Several experiments on animal models showed the safety and efficacy of porous bioactive titanium metal as a synthetic bone under load-bearing conditions. Our preclinical study [26] demonstrated that bioactive treatment effectively enhanced the fusion ability of the porous titanium implants in a canine model of spinal interbody fusion.

Instrumented spinal fusion with autologous iliac crest bone grafting (ICBG) is a gold-standard surgical procedure for the treatment of unstable spinal diseases. However, grafts harvested from the iliac crest are still a major source of autologous bone and the harvesting process is associated with graft site morbidities including residual pain, long operative times and significant blood loss [1].

To accelerate the fusion rate and alleviate donor site problems, several effective osteoinductive agents including recombinant human bone morphogenetic protein-2 (rhBMP-2) and osteogenic protein-1 (OP-1/BMP-7) have been introduced and are widely used clinically [3, 20]. Excellent clinical results have been documented, although some serious adverse effects (AEs) have been reported such as osteolysis around the cage implant, massive bleeding and soft tissue swelling [19, 27, 31]. Porous bioactive titanium metal is not only osteoconductive but also has osteoinductive ability without the need for additional osteogenic cells or agents [10, 25]. Although the osteoinductive ability of porous bioactive titanium metal is limited and the actual mechanism has not been clarified, the osteogenesis it induces is believed to guarantee the high osteoconductive ability of this material.

We conducted a clinical trial of porous bioactive titanium metal for lumbar interbody fusion. Here, we report our preliminary results and discuss the safety and efficacy of porous bioactive titanium metal as one of a new generation of synthetic device materials. This trial was based upon extensive experiments in animal models and clinical success in cementless total hip prosthesis using porous bioactive titanium metal [14, 26].

Methods

Preparation of porous implants

Porous titanium metal was manufactured from a mixture of commercially pure titanium powder <45 μm in particle size (Osaka Titanium Tech. Co. Ltd, Osaka, Japan) and ammonium hydrogen carbonate as spacer particle [32]. Sintering was carried out at 1,400°C for 2 h in Argon gas. Three types of implants, 7, 8 and 9 mm thick and 30 mm wide, were prepared for the clinical trial (Fig. 1). To improve the safety of handling during surgery, a thin outer frame was placed around the porous body and sintered. These implants were supplied by Osaka Yakin Co. (Osaka, Japan). Micro-computed tomography (CT) analysis demonstrated that more than 99% of the porous structures were interconnected and more than 80% of pores were connected through channels more than 52 μm in diameter (Fig. 2). The average porosity was 60% and the average pore size was 250 μm.

Mechanical properties of the porous titanium implants

The compressive strength of the porous titanium body was measured using a universal testing machine (Model EHF-LV020K1-010, Shimadzu Corp., Kyoto, Japan) at a cross-head speed of 1 mm/min. 0.2% yield compressive strength and Young's modulus of a typical 60% porous body were

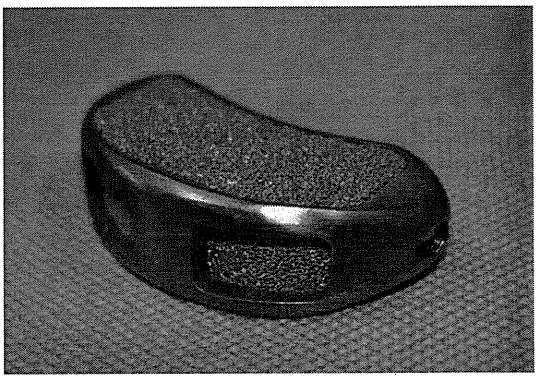

Fig. 1 Photograph of porous bioactive titanium device for transforaminal lumbar interbody fusion

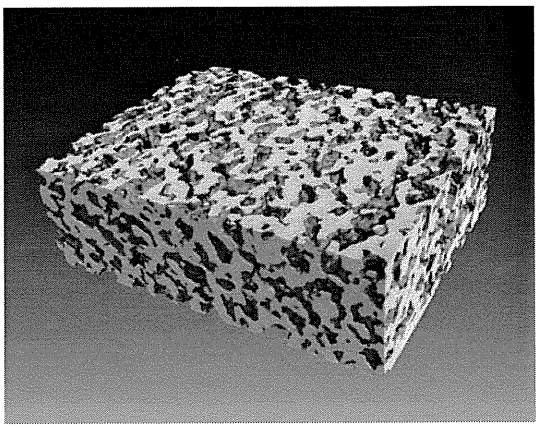

Fig. 2 Micro-computed tomography image showing well-connected internal porous structures

53.0 MPa and 4.2 GPa, respectively. The stiffness was 91.5 kN/m, and this increased to 458.3 kN/m at the outer frame. The porous body combined with the outer frame proved stable against a cyclic load of 10,000 N at 4 Hz for 1,000,000 cycles.

Bioactive surface treatment

The porous implants were treated chemically and thermally to give them a bioactive surface, as described [9, 18]. Briefly, the sintered porous titanium bodies were immersed in 5 M aqueous NaOH solution at 60°C for 24 h, 0.5 mM HCl at 40°C for 24 h, ultrapure water at 40°C for 24 h and then heat-treated at 600°C for 1 h. The homogeneity of the bioactive surface was confirmed by examining the topography and the chemistry of the center and the peripheral parts of several implants using a field emission scanning electron microscope (FE-SEM; Hitachi S-4300, Ibaraki, Japan), an energy-dispersive X-ray microanalyzer (EDX) and X-ray diffractometry (XRD). In vitro apatite-forming ability was confirmed by soaking samples for 3 days in an acellular simulated body fluid (SBF) with ion concentrations (in mM) of Na^+ 142.0, K^+ 5.0, Mg^{2+} 1.5, Ca^{2+} 2.5, Cl^- 147.8, HCO_3^- 4.2, HPO_4^{2-} 1.0 and SO_4^{2-} 0.5: nearly equal to those of human blood plasma at 36.5°C and prerequisite conditions for generating bioactive materials [17]. The implants were sterilized by 25 kGy γ-radiology exposure before surgical implantation.

Evaluation of implants

All devices with the same lot number destined for clinical use were analyzed in vitro before implantation. All parameters of mechanical strength including yield compressive strength, elastic modulus and fatigue strength were within an error of <5%. Mechanical testing found no failure of the device, nor any loss of titanium particles. FE-SEM, EDX and XRD studies confirmed the homogeneity of the bioactive surface both centrally and peripherally. After the surface treatment, the whole porous surface was uniformly changed to a bioactive thin TiO2 layer approximately 1 μm thick with sub-micron-sized pores. The walls of the porous body were completely covered with apatite within 3 days of soaking in SBF, indicating that the whole surface of the implant could be rendered bioactive by the chemical and thermal treatments (Fig. 3a–c).

Transforaminal lumbar interbody fusion (TLIF) [11]

All surgical procedures were performed by the two senior authors (S.F. and M.T.).

Following a midline skin incision, the lateral aspect of facet joints was exposed through a midline subperiosteal approach or Wiltse's approach depending on the case. After bilateral pedicle screw placement, the neural foramen was exposed by excision of the ipsilateral facet joint. Disc space preparation with the removal of degenerative disc materials and cartilaginous endplate was performed carefully from the safety triangle zone between the exiting and traversing nerve roots. In the case of concomitant spinal canal stenosis, neural decompression was done using a surgical microscope. The bioactive porous titanium implant was placed into the intervertebral space through the opened safety triangle zone and small local bone chips were packed around the implant as monitoring bone material. Compressive force was applied through the pedicle screws and pre-bent rods were set on the screws bilaterally. The patients were allowed to walk while wearing a hard brace beginning on the first day after surgery.

Patients

This was a prospective clinical case series on five patients (3 men and 2 women) with degenerative unstable lumbar

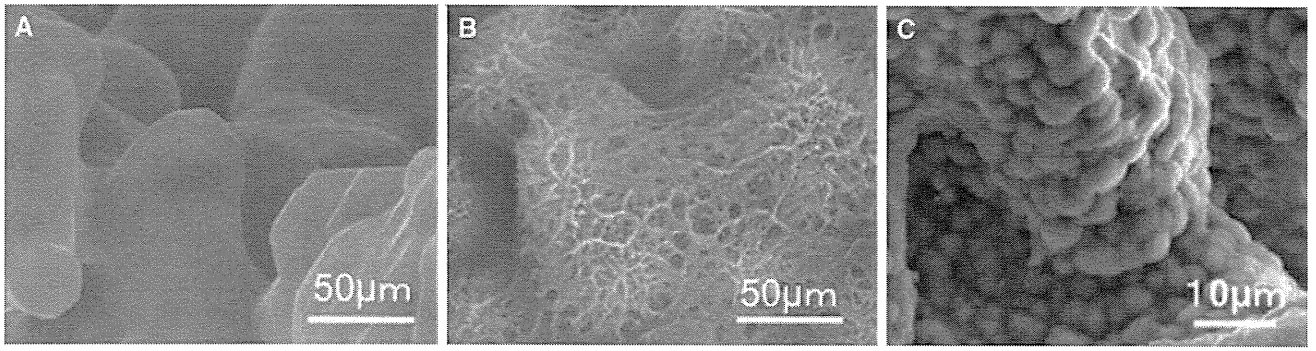

Fig. 3 Field emission scanning electron microscope (FE-SEM) images showing surface morphological changes to the porous titanium metal. **a** Before treatment, the surface was smooth. **b** After chemical and thermal treatment, a thin submicron-sized pore layer was formed on the surface. **c** Apatite formation on the whole surface of the porous bioactive titanium metal after soaking in simulated body fluid (SBF) for 3 days

lesion who were eligible for surgical treatment and who were referred to our University Hospital from November 2008 to June 2009. In all cases, the patient and his or her relatives were informed about the benefits and the risks of the implant. Written informed consent was obtained from all patients and/or their relatives, in accordance with protocols approved by our Institutional Ethics Committee and in agreement with the Declaration of Helsinki.

Among the five patients enrolled there were three with degenerative spondylolisthesis and two with isthmic spondylolisthesis. Inclusion criteria for this preliminary clinical trial were symptomatic single-level unstable lumbar disc disease with or without compression of neural elements, which were refractory to adequate conservative treatments for at least 3 months preoperatively. Patients with multilevel diseases, a previously operated spine, osteoporosis, general inflammatory disease or a severe comorbidity such as cardiovascular disease or renal dysfunction were excluded. The average age of the enrolled patients at surgery was 51.6 years (range 36–61 years).

Clinical assessment

A patient self-assessed 100 mm visual analog scale (VAS) (0 mm = no pain, 100 mm = worst pain imaginable) for both low back pain (LBP) and leg pain (LP), the Japanese Orthopaedic Association (JOA) score (Table 1) and its recovery rate [recovery rate = postoperative score − preoperative score/29 (full score) − preoperative score × 100 (%)] were examined before operation and postoperatively. A self-assessed patient's satisfaction score was examined after the surgery. For subjective assessment of the overall results of surgery, the patient was asked to select from among the options: very satisfied, satisfied, somewhat satisfied, somewhat dissatisfied or dissatisfied. The satisfaction score was recorded as a score at all time points. All patients complained of LBP preoperatively and four complained of concomitant LP. The average preoperative JOA score was 15.8 (range 11–21). The average preoperative VAS values for LBP and LP were 37.6 mm (range 10–50 mm) and 21.4 mm (range 0–60 mm), respectively. An independent expert nurse carried out the assessment of pre- and postoperative VAS and the patient's satisfaction score. The JOA scores and VAS measures were analyzed statistically using paired *t*-tests and $P < 0.05$ was considered statistically significant.

Radiological assessment

Magnetic resonance imaging (MRI), multidetector-row computed tomography (MDCT) and lateral dynamic X-rays were used to assess the neural compression and

Table 1 JOA score classifications for low-back pain

Parameter	JOA score
Subjective symptoms	9
Low-back pain	
None	3
Occasional mild pain	2
Frequent mild or occasional severe pain	1
Frequent or continuous severe pain	0
Leg pain and/or tingling	
None	3
Occasional slight symptoms	2
Frequent slight or occasional severe symptoms	1
Frequent or continuous severe symptoms	0
Gait	
Normal	3
Able to walk >500 m, although it causes pain, tingling, and/or muscle weakness	2
Unable to walk >500 m due to leg pain, tingling, and/or muscle weakness	1
Unable to walk >100 m due to leg pain, tingling, and/or muscle weakness	0
Clinical signs	6
Straight leg-raising test (including tight hamstrings)	
Normal	2
30–70°	1
<30°	0
Sensory disturbance	
None	2
Slight disturbance (not subjective)	1
Marked disturbance	0
Motor disturbance	
Normal (Grade 5/5)	2
Slight weakness (Grade 4/5)	1
Marked weakness (Garde 0–3/5)	0
Restriction of ADL	14
ADL (restriction)	
Turning over while lying down	
Standing	
Washing	
Leaning forward	
Sitting (~1 h)	
Lifting/holding heavy objects	
Walking	
Urinary bladder function	−6
Normal	0
Mild dysuria	−3
Severe dysuria (incontinence, urinary retention)	−6

JOA Japanese Orthopaedic Association

ADL activities of daily living

For each activity of daily living category severe restriction was accorded a score of 0; moderate restriction, a score of 1; and no restriction, a score of 2

dynamic situation. Preoperative dynamic lateral X-rays showed marked segmental instability in all five patients. To assess bony union postoperatively, lateral dynamic radiographs were obtained at 3, 6 and 12 months. More than 3° motion on flexion–extension was considered to indicate nonunion. In addition, radiolucent regions around the pedicle screws and the implant were defined as showing nonunion. To evaluate the placement of implant and pedicle screws, bony union and AEs, coronal and sagittal reconstruction views using MDCT were assessed at 1 week and at 1, 3, 6 and 12 months after surgery. Bony union was defined as complete when there was osseous continuity between bony endplate and implant on both the coronal and sagittal MDCT images. Nonunion was defined as the presence of a visible gap between the vertebral endplate and implant, or radiolucency around the pedicle screws. Successful bony union was recorded when the assessments of aforementioned radiological parameters were complete. A change of 3 mm or more of implant migration into the vertebral endplate was defined as significant subsidence. MRI was performed at 1 week and at 1, 3, 6 and 12 months after surgery to assess neural decompression and dural tube extension, any AEs including inflammatory reaction around the implant such as vertebral endplate erosion, Modic change [20] and any fluid collection. Three independent experienced spinal surgeons, each with at least 10 years of experience, did all the radiological assessments. Each patient's preoperative clinical and radiological data are summarized in Table 2.

Ethical considerations

The study was performed in accordance with the principles of the Declaration of Helsinki and of Good Clinical Practice and was registered on the University Hospital Medical Information Network Clinical Trials Registry (UMIN00000 1448). Approval was obtained from the relevant competent authorities and our institutional Committee of Ethics before the trial began. As clinicians, the authors played a leading role in this new type of clinical trial, which is extremely rare in the development of new medical devices in Japan. We prepared all the protocols of this study by ourselves and were supported by a translational research center in Kyoto University. The independent clinical research coordinator of the translational research center managed all clinical data, which were extracted from each patient's clinical research form. The endpoints of this clinical trial were achievement of good clinical results, bony union, no serious AEs and avoidance of the need for autologous ICBG.

Results

Clinical results

In all five patients, the preoperative LBP and radicular symptoms were resolved immediately after the operation. No surgery-related neurological deficit or wound breakdown was observed in any patient. The mean operating time was 164.6 min (range 154–179 min) and the mean estimated intraoperative blood loss was 192 mL (range 80–310 mL). No patient required transfusion or ICBG. No surgery-related complication was observed. The mean follow-up period was 15.2 months (range 12–19 months). The average postoperative JOA score was 25.6 at 1 month, 25.6 at 3 months, 27 at 6 months and 26.6 at 12 months (range 18–29). The mean recovery rate of the JOA score was 76.6% at 1 month, 77.5% at 3 months, 88.0% at 6 months and 85.8% at 12 months (range 38.9–100%). The postoperative JOA score improved significantly compared with the preoperative score at all times ($P = 0.002$ at 12 months). The mean VAS was 2 mm at 1 month, 2 mm at 3 months, 6 mm at 6 months and 2 mm at 12 months (range 0–30 mm) for LBP. It was 0 mm at 1 month, 0 mm at 3 months, 4 mm at 6 months and 2 mm at 12 months (range 0–20 mm) for LP. Both VAS measures were significantly improved compared with preoperative scores at all times (at 12 months; LBP $P = 0.027$; LP $P = 0.012$). All but one patient satisfied very much through the experiment periods. All clinical parameters showed rapid recovery within 1 month, which indicated a low level of invasiveness and good stabilization of the surgery (Fig. 4).

Table 2 Summary of preoperative patient's demographic data

Case	Age	Sex	Diagnosis	Level	Symptoms	Pre JOA	Pre VAS (LBP)	Pre VAS (LP)
1	54	F	DS	L4/5	LBP + LP	21	10	60
2	36	M	IS	L5/S	LBP + LP	12	80	50
3	51	F	DS	L4/5	LBP	19	80	0
4	61	F	DS	L4/5	LBP + LP	11	60	60
5	56	M	IS	L5/S	LBP + LP	16	50	20

DS degenerative spondylolisthesis, *IS* isthmic spondylolisthesis, *LP* leg pain, *LBP* low back pain, *VAS* visual analog scale